ANALYSIS OF CLAY CONSOLIDATION BY RATE PROCESS THEORY

Thesis for the Degree of M. S.

MICHIGAN STATE UNIVERSITY

Robert J. Neukirchner

1965

ABSTRACT

ANALYSIS OF CLAY CONSOLIDATION
BY RATE PROCESS THEORY

by Robert J. Neukirchner

The consolidation of clay is composed of two processes; the first is drainage of excess pore water to reduce pore pressures and the second involves the deformation of the clay particle structure. In this thesis the deformation phenomenon is considered to occur through the breaking and reforming of bonds at the clay particle contacts and is assumed to be governed by the rate process theory. A rheological model is proposed which represents the behavior of the clay structure under load. The model parameters are related to properties of the clay structure and the parameters are used to evaluate the deformation charactertistics of the clay structure.

ANALYSIS OF CLAY CONSOLIDATION BY RATE PROCESS THEORY

By

Robert J. Neukirchner

A THESIS

Submitted to
Michigan State University
in partial fulfillment of the requirements
for the degree of

MASTER OF SCIENCE

Department of Civil Engineering

1965

ACKNOWLEDGMENTS

The writer is indebted to his major professor, Dr. T. H. Wu, Professor of Civil Engineering, for his everpresent aid, guidance and encouragement throughout the writer's graduate program and during the preparation of this thesis. Thanks also to Dr. A. K. Loh and J. R. Adams for their helpful suggestions and criticisms, and to Professor D. Resendiz of the University of Mexico for supplying the time-consolidation data on the Mexico City clays.

Thanks are due also to the Civil Engineering Department of Michigan State University for the financial assistance which made the completion of these studies possible.

TABLE OF CONTENTS

LIST OF FIGURES

NOTATION

A - Slope parameter

C - Constant

C_v - Coefficient of consolidation

h - Boltzmann's constant

k - Planck's constant

k_1, k_2 - rheological model parameters

K, L, M, N - constants with respect to time

$\bar{p}_o$ - applied pressure increment

$\bar{p}$ - total effective stress on the model

$\bar{p}_1$ - effective stress on the flowing bonds

R - gas constant

T - absolute temperature

t - time

tp - time for 100% primary consolidation to occur determined according to log time method

U - axial deformation

U^* - percent total axial deformation

U^{**} - dimensionless strain used in Case I solution

U_o, U_∞ - initial and final values of axial deformation

$Z(t)$ - time parameter

$\left.\begin{matrix}\alpha \\ \beta\end{matrix}\right\}$ - rate process theory parameters

γ, γ_1 - deformations of model (shear strain)

γ_{oct} - octahedral shear strain

$\epsilon_1, \epsilon_2, \epsilon_3$ - principal strains

$(\epsilon_1)_o, (\epsilon_1)_\infty$ - initial and final values of strain, ϵ_1

λ - average distance between interparticle bonds

λ_1 - distance between adjacent planes of slip

ν - number of flowing particle contacts per unit area

$\sigma_1, \sigma_2, \sigma_3$ - principal stresses

σ_{oct} - octahedral normal stress

τ - shear stress

τ_r - shear stress in flowing bonds

τ_{oct} - octahedral shear stress

CHAPTER I

INTRODUCTION

The reduction in volume with time under a constant applied load is called consolidation. Consolidation of clay has customarily been considered to consist of two distinct parts; a primary and a secondary part. With reference to primary consolidation, Terzaghi and Peck (1948) say, "The gradual decrease of the water content at constant load is known as consolidation." The rate of primary consolidation is considered to be governed by the velocity of the flow of water from the material under a hydraulic gradient.

The "secondary time effect" is described by the same authors as " . . . due to the gradual adjustment of the soil structure to stress, combined with the resistance offered by the viscosity of the adsorbed layers to a slippage between grains."

The primary phase is considered to be adequately described by the flow of water from the voids under a hydraulic gradient and was solved by Terzaghi's one-dimensional consolidation theory. Secondary consolidation, however, cannot be attributed to the hydraulic phenomenon, and may continue for long periods after the excess hydrostatic pressure has approached zero. In an effort to determine the nature of this phenomenon, several authors (Altschaffel, Gibson and Lo, Leonards, Tan, Schiffmann and others) have proposed rheological models designed to describe clay consolidation.

In recent studies on clay deformation in general, the rate process theory of Eyring et al (1948) has been used to describe the mechanism of slip at interparticle contacts. The result of these investigations seems to give a satisfactory insight into the nature of deformation of clay.

Christensen and Wu (1964) and Muryama and Shibata (1964) analyzed creep and stress relaxation in clay by the rate process theory. They also proposed a rheological model consisting of a parallel arrangement of a spring, and a spring and a dashpot to approximate the deformation of the clay structure under creep. The results of this analysis agreed well with test data.

Considering that consolidation of clay also involves contact slips and is a special case of clay deformation, the author has used the model of Christensen and Wu to describe this phenomenon. The solution is generalized to take into account the stress changes in the system during primary consolidation.

This approach is considered because it seems reasonable to expect that one mechanism rather than two distinct processes should be used to represent clay consolidation. In addition, the rate process theory offers an opportunity to study the mechanism of clay deformation.

CHAPTER II

THEORY

It is commonly held that clay particles are thin, plate-like structures with a high surface area to volume ratio. Tan (1953) (also Rosenquist, 1959, and Mitchell, 1964,) has proposed that these particles form edge to face contacts resulting in a continuous clay structure.

The nature of these contacts and the bonding forces at the contacts are still the subject of much disagreement. However, deformation of the clay structure under an applied load is considered to be the result of slip at these particle contacts due to local stresses. On the molecular level this involves a continuous breaking and reforming of bonds at the contacts (Christensen and Wu, 1964, and Mitchell, 1964) and is considered to be a rate process. It should be mentioned that a wide range in bond strengths may be encountered in deformation. Some contacts break under the smallest stress while others remain intact until shear failure of the soil occurs.

The deformational properties of the particle structure of a clay can be approximately represented by the rheological model shown in figure 1.

The spring k_2 represents the behavior of the non-flowing bonds in the clay structure under stress $\overline{\tau}$. These bonds are assumed to behave elastically under stress. The right hand side of the model accounts for the effects of the flowing bonds. The bonds at any particular contact are considered to have a specific bond strength. When the applied stress exceeds

this strength flow occurs at the contact. Once flow is initiated the bond may be broken or reestablished depending on the contact displacement. Bonds are distinct from particle contacts as there may be many bonds at a single contact. The flow is assumed to obey the rate process theory.

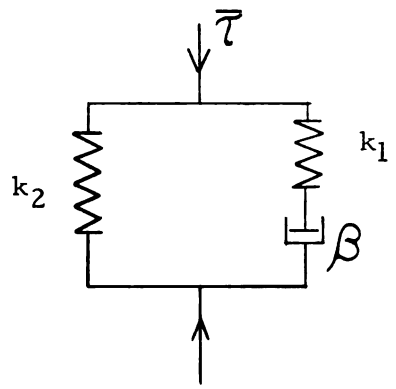

Figure 1. Proposed rheological model

Considering the behavior of the model under an applied stress $\bar{\tau}$, the combined resistance of k_1 and k_2 account for the initial deformation which represents the elastic response of the structure. As deformation proceeds stress is transferred from the weaker contacts, which flow, to the stronger, non-flowing contacts. In the model, as the dashpot flows, the stress is transferred to the left half of the model until ultimately all the stress resides in spring k_2. Then the flow ceases.

Experiments show that this model satisfactorily represents the major deformational characteristics observed in clays.

Under an applied stress $\bar{\tau}$ the stress in the left-hand side of the model is

$$\bar{\tau} - \tau_r = k_2 \gamma \qquad (1)$$

where τ_r is the stress in the right side of the model and γ is the total shear strain. In the right half, the stress is

$$\tau_r = k_1 (\gamma - \gamma_r) \tag{2}$$

If we consider the viscous flow in the dashpot to behave according to the rate process theory we have (according to Glasstone, Laidler, and Eyring, 1941)

$$\dot{\gamma} = \frac{d\gamma}{dt} = \beta \sinh \alpha \tau_r + \frac{d\tau_r}{dt} \frac{1}{k_1} \tag{3}$$

where

$$\alpha = \frac{\lambda}{2\nu kT}$$

$$\beta = 2 \frac{\lambda}{\lambda_1} \frac{kT}{h} \exp(-\Delta F/RT)$$

and

k = Botlzmann's constant;

T = absolute temperature;

h = Planck's constant;

R = gas constant;

ΔF = Activation energy;

λ = average jump distance;

λ_1 = distance between planes of slip;

ν = number of flowing contacts

From eq. (1)

$$\dot{\gamma} = \frac{d\gamma}{dt} = \frac{1}{k_2} (\dot{\bar{\tau}} - \dot{\tau}_r) \tag{4}$$

Combining eqs. (3) and (4) we get

$$\frac{k_1 + k_2}{k_1 k_2} \frac{d\tau_r}{dt} = \frac{1}{k_2} \frac{d\bar{\tau}}{dt} - \beta \sinh \alpha \tau_r \tag{5}$$

which is the differential equation governing the deformation of our model.

As proposed, the model represents the behavior of the clay structure under load but does not take into account the presence of the pore water pressure. In a clay-water system the load on the soil skeleton is the effective stress, which in a consolidation test increases with decreasing pore pressure. If we consider the stress under a given axial stress increment p_o

$$p_o = p_w + \bar{p} \tag{6}$$

in which p_w is pore water pressure and $\bar{p}$ is effective axial stress.

From the Terzaghi one-dimensional consolidation theory we have

$$\text{at } t=0 \quad , \quad p_w = p_o$$

$$\text{at } t=t_p \quad , \quad p_w = 0$$

where t_p represents the time for 100% primary consolidation as determined graphically from a time-consolidation curve.

Rewriting (6) we have

$$\bar{p} = p_o - p_w \tag{6a}$$

which implies

$$\text{at } t=0 \quad , \quad \bar{p}=0$$

$$\text{at } t=t_p \quad , \quad \bar{p}=p_o$$

The change in p_w and $\bar{p}$ are given by the theory of consolidation (Terzaghi, 1923).

Graphically this can be shown by figure 2.

From this it is seen that $\bar{p}$ represents the loading condition on the soil structure (the model) and we note that for

$$0 < t < tp \quad , \quad \bar{p} = \bar{p}(t), \quad \dot{\bar{p}} \neq 0$$

$$t < tp \quad , \quad \bar{p}=\text{constant}, \quad \dot{\bar{p}} = 0$$

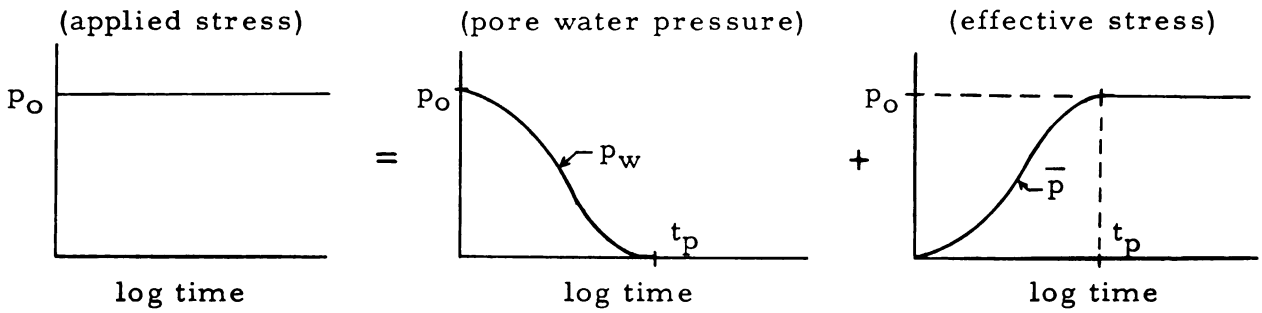

Figure 2. Loading conditions for general model

If we consider the deformation that occurs after time $t > t_p$, $\bar{p}$ is constant. We may apply the condition $\frac{d\bar{\tau}}{dt} = 0$ to eq. (5), which yields

$$\frac{k_1 + k_2}{k_1 \; k_2} \quad \frac{d\,\tau_r}{dt} = -\beta \sinh \alpha \tau_r \qquad (7)$$

or

$$\frac{d(\alpha \tau_r)}{d\left(\alpha \frac{k_1 k_2}{k_1 + k_2} t\right)} = -\beta \sinh \alpha \tau_r \qquad (8)$$

Writing $\sinh \alpha \tau_r = \frac{e^{\alpha \tau_r} - e^{-\alpha \tau_r}}{2}$ and substituting this into (8) we get:

$$\frac{d\,(\alpha \tau_r)}{d\left(\alpha \frac{k_1 k_2}{k_1 + k_2} t\right)} = \frac{-\beta}{2} \left(e^{\alpha \tau_r} - e^{-\alpha \tau_r}\right) \qquad (9)$$

Upon integration,

$$\tau_r = -\frac{1}{\alpha} \ln \tanh \left[\frac{1}{2} \alpha \beta \frac{k_1 \; k_2}{k_1 + k_2} t - C\right] \qquad (10)$$

If we consider the load $\bar{\tau}$ applied instantaneously, then

at $t = 0$ $\quad \tau_r = \frac{k_1}{k_1 + k_2} \bar{\tau}$ ($\bar{\tau}$ = a constant)

so that

$$C = -\frac{2\ (k_1 + k_2)}{\alpha\beta k_1 k_2} \quad \tanh^{-1} \exp\left(-\frac{\alpha k_1 \bar{\tau}}{k_1 + k_2}\right)$$

from which

$$\tau_r = -\frac{1}{\alpha} \quad \ln \tanh\left[\frac{1}{2}\alpha\beta\frac{k_1 k_2}{k_1 + k_2} t + \tanh^{-1}\exp\left(-\frac{\alpha k_1 \bar{\tau}}{k_1 + k_2}\right)\right] \quad (11)$$

From eq. (1)

$$\gamma = \frac{1}{k_2} \quad (\bar{\tau} - \tau_r)$$

Substituting (11) into (1) we have

$$\gamma = \frac{1}{k_2}\bar{\tau} + \frac{1}{\alpha k_2} \quad \ln \tanh\left[\frac{1}{2}\alpha\beta\frac{k_1 k_2}{k_1 + k_2} t + \tanh^{-1}\exp\left(\frac{\alpha k_1 \bar{\tau}}{k_1 + k_2}\right)\right] \quad (12)$$

Thus the deformation of our model is governed by two cases.

Case I - for $t < t_p$; $\bar{\tau} = \bar{\tau}(t)$

The general equation (eq. 5) holds.

Case II - for $t > t_p$; $\bar{\tau} = \text{const.}$; $\frac{d\bar{\tau}}{dt} = 0$

The deformation is given by eq. (12).

CHAPTER III

EXPERIMENTAL PROGRAM

The purpose of the experimental program is to compare the observed behavior of the soils tested with the theoretical predictions. Further, evaluation of the significance of the model parameters will be in order if test data and the model behavior are in agreement.

Clays Tested - Time-deformation curves were obtained on three different types of clay. The author conducted tests on two types of glacial lake clays.

The specimens consist of remolded samples of a glacial clay from a site approximately 15 miles south of Sault Ste. Marie, Michigan, and undisturbed and remolded samples of a glacial clay from Marine City, Michigan.

Data on the Mexico City clay were provided by Professor D. Resendiz of the University of Mexico.

The index properties of the glacial clays tested are shown in fig. 4.

Testing Procedure - All samples were tested with standard consolidation test equipment. The samples are two and one-half inches in diameter with an original height of 1.00 inches.

Clay	LL	PL	Pl	Clay Fraction %
Marine City #1	46.8	24.1	23.7	-
Marine City #2	41.4	21.7	19.7	68
Sault Ste. Marie	60.5	23.6	36.2	60

Figure 3. Index properties of clays used

Loading increments varied throughout the testing sequence and are given with other pertinent information for each test in Appendix A.

Wherever possible each load increment was maintained until deformations stopped. As can be seen from the test data, the tests extended over long periods and many had to be stopped before the final deformation was reached because of time considerations.

The shortest time duration of a load increment was 4 days, while several tests lasted for more than 100 days and one was terminated after 253 days.

On such long-term tests, the effects of temperature variations and other minor disturbances are readily apparent; however these effects are, in most cases, short term and do not seriously affect the long-term behavior of the clays.

Test results and calculations of parameters are shown in Appendix C. Time-consolidation curves for each load increment are shown graphically in Appendix B.

CHAPTER IV

CALCULATION OF MODEL PARAMETERS

In order that deformation equations (5) and (12) for the proposed model may be used to analyze the results of the experimental program we must first adopt a consistent and convenient method for calculating our model parameters k_1, k_2, α and β .

Let us define τ and γ in eqs. (5) and (12) as the effective shear stress and shear strain on octahedral plane in our stress system.

$$\tau_{oct} = \frac{1}{3}\sqrt{(\bar{\sigma}_1-\bar{\sigma}_2)^2+(\bar{\sigma}_2-\bar{\sigma}_3)^2+(\bar{\sigma}_3-\bar{\sigma}_1)^2} \tag{13}$$

and

$$\gamma_{oct} = \frac{2}{3}\sqrt{(\epsilon_1-\epsilon_2)^2+(\epsilon_2-\epsilon_3)^2+(\epsilon_3-\epsilon_1)^2} \tag{14}$$

where $\sigma_{1,2,3}$ are major, intermediate and minor principal stresses and $\epsilon_{1,2,3}$ are the major, intermediate and minor principal strains.

In a consolidation test we have the conditions that

$$\begin{cases} \bar{\sigma}_2 = \bar{\sigma}_3 & (15) \\ \epsilon_2 = \epsilon_3 = 0 & (16) \end{cases}$$

Putting (15) into (13) gives us:

$$\tau_{oct} = \frac{1}{3}\sqrt{(\bar{\sigma}_1-\bar{\sigma}_3)^2+(\bar{\sigma}_3-\bar{\sigma}_1)^2} \tag{17}$$

The stress $\bar{\sigma}_3$ is indeterminate for a consolidation test but a good assumption is that

$$\bar{\sigma}_3 = k_o\bar{\sigma}_1 = k_oP_o \tag{18}$$

where k_o is the at rest coefficient of earth pressure.

k_o can be evaluated by the equation

$$k_o = 1 - \sin \bar{\phi} \tag{19}$$

where $\bar{\phi}$ represents the angle of internal friction in terms of effective stress (Bishop, 1958). For the clays studied, an average value of $\bar{\phi}$ is 30^o; therefore

$$k_o = 1 - \sin 30^o = 0.5 \tag{20}$$

Substituting (20) and (18) into (13) our expression becomes

$$\tau_{oct} = \frac{1}{3}\sqrt{2\left(\frac{\bar{\sigma}_1}{2}\right)^2} = \frac{p_o}{3\sqrt{2}} \tag{21}$$

where p_o is the increment in consolidation pressure applied. At $t>tp$, the entire load is carried by the effective stress and

$$\bar{p} = p_o$$

Now if we turn to our equation for octahedral shear strain and put (16) into eq. (14) we get

$$\gamma_{oct} = \frac{2}{3}\sqrt{(\epsilon_1)^2+(\epsilon_1)^2} = \frac{2\sqrt{2}}{3}\epsilon_1 \tag{22}$$

Let us now consider the two conditions for the deformation of the model separately. Beginning with Case II, the condition $\dot{\bar{\tau}} = 0$ gives us

$$\gamma = \frac{1}{k_2}\bar{\tau} + \frac{1}{\alpha k_2} \ln \tanh\left[\frac{1}{2}\alpha\beta\frac{k_1 k_2}{k_1+k_2} t + \tanh^{-1}\exp\left(\frac{-k_1\alpha\bar{\tau}}{k_1+k_2}\right)\right] \tag{12}$$

Substituting (21) and (22) into (12) we have

$$\epsilon_1 = \frac{p_o}{4k_2} + \frac{3}{2\sqrt{2}\alpha k_2} \ln \tanh\left[\frac{1}{2}\alpha\beta\frac{k_1 k_2}{k_1+k_2} t + \tanh^{-1}\exp\left(\frac{-\alpha k_1 p_o}{3\sqrt{2}(k_1+k_2)}\right)\right] \tag{23}$$

For purposes of analyzing the test results, eq. (23) would be much more valuable if it were written in a dimensionless form. Consider the following:

$$\text{at} \quad t=0 \qquad (\epsilon_1)_i = \frac{1}{4}\frac{p_o}{k_1+k_2} \tag{24}$$

where $(\epsilon_1)_i$ is the elastic response (instantaneous) to the applied stress.

$$\text{at} \quad t=\infty \qquad (\epsilon_1)_\infty = \frac{1}{4}\frac{p_o}{k_2} \tag{25}$$

We now propose a dimensionless strain U** such that

$$U^{**} = \frac{\epsilon_1 - (\epsilon_1)_i}{(\epsilon_1)_\infty - (\epsilon_1)_i} \tag{26}$$

Making use of conditions (24) and (25), we may write eq. (23) in the form:

$$U^{**} = 1 + \frac{3\sqrt{2}}{p_o}\left(\frac{k_1+k_2}{k_1}\right)\frac{1}{\alpha}\ln\tanh\left[\frac{1}{2}\alpha\beta\frac{k_1k_2}{k_1+k_2}t + \tanh^{-1}\exp\left(-\frac{\alpha k_1 p_o}{3\sqrt{2}(k_1+k_2)}\right)\right] \tag{27}$$

or

$$U^{**} = 1 + \frac{1}{A}\ln\tanh\left[Z(t)+\tanh^{-1}\exp(-A)\right] \tag{28}$$

where

$$\left.\begin{aligned} A &= \frac{\alpha k_1 p_o}{3\sqrt{2}(k_1+k_2)} \\ Z(t) &= \frac{1}{2}\alpha\beta\frac{k_1k_2}{k_1+k_2}t \end{aligned}\right\} \tag{29}$$

We can now make use of the fact that eq. (28) expresses U** as a function of Z(t) and can plot solutions of the equation in the form of U** vs. Z(t) for different values of A. The solutions in this form are shown in figure 4.

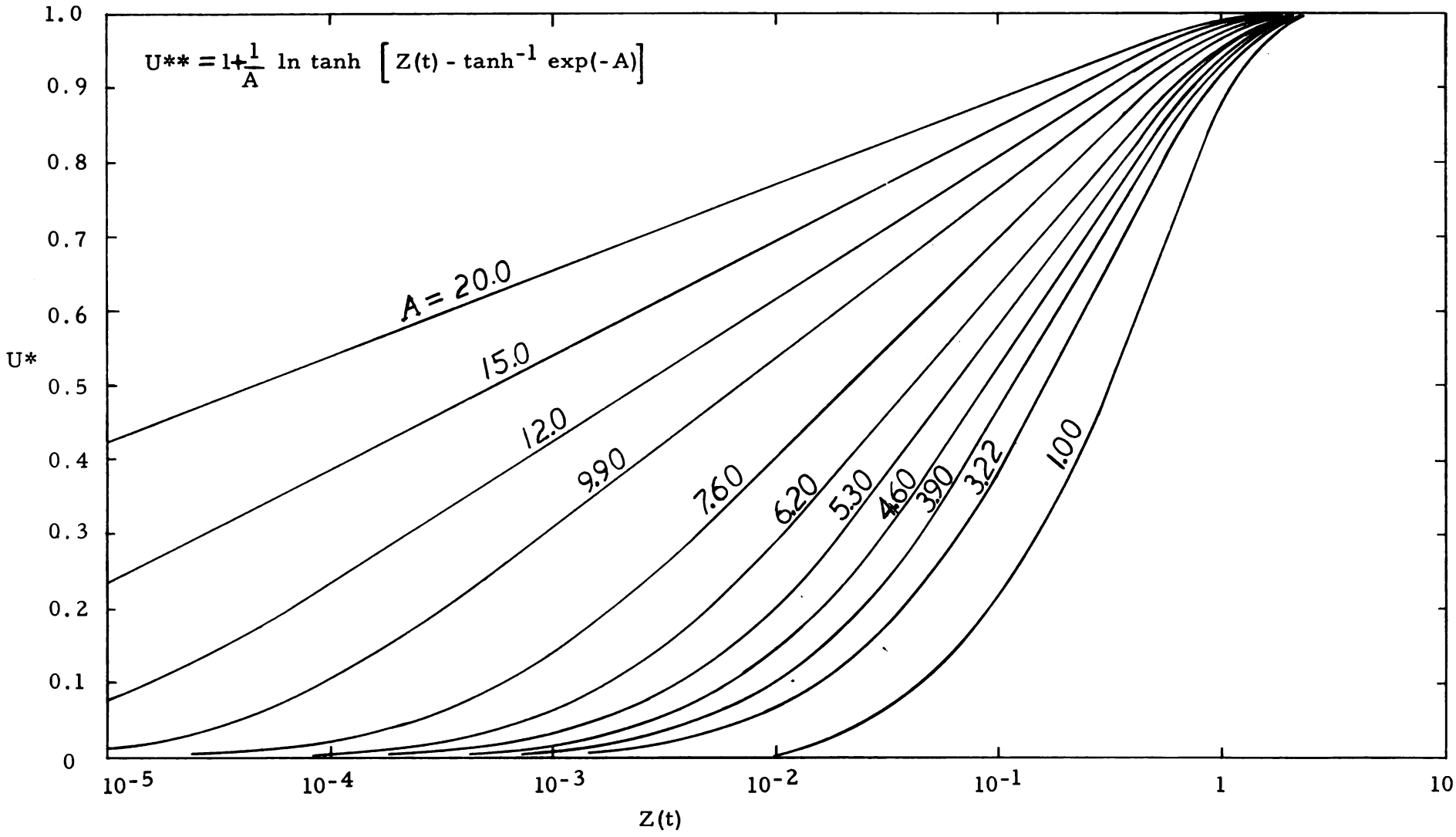

Figure 4. Graphical Solutions for Case II

To relate the curves of figure 4 to the consolidation data we define a parameter

$$U^* = \frac{(\epsilon_1)}{(\epsilon_1)_\infty} = \frac{U_1}{U_0} \tag{30}$$

where U represents axial deformation.

A graph showing U* vs. Z(t) for $\frac{d\bar{\tau}}{dt} = 0$ (case II) would appear as shown in figure 5.

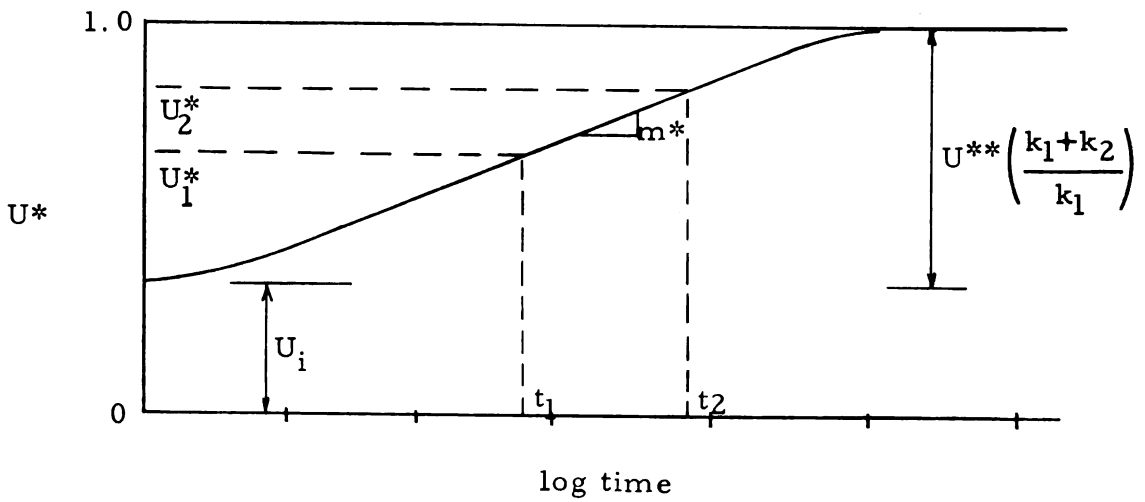

Figure 5. Relation of U* to U** curves

From figure 5, U* is related to U** by the equation

$$U^{**} = \frac{U^* - U_i}{1 - U_i} \tag{31}$$

where $U_i = \frac{(\epsilon_1)_i}{(\epsilon_1)_\infty} = \frac{p_o}{4(k_1+k_2)} \Big/ \frac{p_o}{4k_2} = \frac{k_2}{k_1+k_2}$ (31a)

As shown, the slope of the straight portion of the curve is given by slope m* where

$$m^* = \frac{U_2^* - U_1^*}{\log t_2 - \log t_1}$$

The corresponding slope of the U** curve in figure 4 is given by m** where

$$m^{**} = \frac{U_2^{**} - U_I^{**}}{\log Z(t)_2 - \log Z(t)_1}$$

For the same time differences we have the relationship that

$$m^{*} = (m^{**}) \frac{1}{1-U_i} = m^{**} \frac{(k_1+k_2)}{k_1} \qquad (32)$$

Therefore for a given curve of U* vs t we can evaluate the slope m* , calculate m** by eq. (32) and then obtain a value of A which gives the best fit to m** from figure 4. We note that the initial conditions of eq. (28) differ from that in the consolidation test. However, we restrict the use of eq. (28) through (32) to the range $t \succ t_p$. Hence, the initial conditions do not effect the eqs. in this range.

All the calculations require that we have a quantity $(\epsilon_1)_\infty$. This value of ultimate deformation, $(\epsilon_1)_\infty$, may be obtained by letting each test run until an equilibrium is reached. However, waiting for the deformations to stop in a consolidation test is often impractical as the time required may be extremely long.

We can however compute the value of ultimate deformation, or at least an estimate of this value from the following relationships.

The variation of the strain rate with increasing strain is

$$\frac{d\dot{\epsilon}}{d\epsilon} = \frac{d\dot{\epsilon}}{dt} \cdot \frac{dt}{d\epsilon} \qquad (33)$$

Now we take eq. (25) and express it as

$$\epsilon_1 = K + L \ln \tanh (Mt + N) \qquad (34)$$

Taking the first derivative we get

$$\frac{d\epsilon_1}{dt} = 2LM \operatorname{csch} 2(Mt+N) \tag{35}$$

Differentiating again yields

$$\frac{d\dot{\epsilon}_1}{dt} = \frac{-4LM^2 \operatorname{csch} 2(Mt+N)}{\tanh 2(Mt+N)} \tag{36}$$

from which

$$\frac{d\dot{\epsilon}}{d\epsilon} = -2M \operatorname{ctnh} 2(Mt+N) \tag{37}$$

We see that if $(Mt+N) \rightarrow \infty$ as $t \rightarrow \infty$, then $\operatorname{ctnh} 2(Mt+N) \rightarrow 1$. Therefore, for large values of t

$$\frac{d\dot{\epsilon}}{d\epsilon} = -2M \tag{38}$$

Thus an arithmetic plot of $\dot{\epsilon}$ vs. ϵ for large t has a constant slope of -2M. The intercept of this curve at $\dot{\epsilon}=0$ gives $(\epsilon_1)_\infty$ as the ultimate deformation.

Note also that equation (38) gives us another equation for $\alpha\beta$ in that

$$\frac{d\dot{\epsilon}}{d\epsilon} = -2M = -\alpha\beta \frac{k_1 k_2}{k_1+k_2} \tag{39}$$

With $(\epsilon_1)_\infty$ known, the value of k_2 can be calculated from eq. (25).

To evaluate k_1 we must turn our attention to case I. For this case the deformation of the model for $t < tp$ is governed by the general equation

$$\frac{k_1+k_2}{k_1 k_2} \frac{d\tau_r}{dt} = \frac{1}{k_2} \frac{d\bar{\tau}}{dt} - \beta \sinh \alpha \tau_r \tag{5}$$

To be consistent with our analysis of case II we consider τ_r and $\bar{\tau}$ as stresses on the octahedral plane. Using (21) and letting $\bar{\sigma}_1 = \bar{p}$ we may rewrite (5) as

$$\frac{k_1+k_2}{3\sqrt{2}k_1k_2}\quad\frac{d\bar{p}_1}{dt}=\frac{1}{3\sqrt{2}k_2}\left(\frac{d\bar{p}}{dt}\right)-\beta\sinh\left(\frac{\alpha}{3\sqrt{2}}\right)\bar{p}_1$$

or

$$\frac{d\bar{p}_1}{dt}=\frac{k_1}{k_1+k_2}\frac{d\bar{p}}{dt}-\frac{3\sqrt{2}k_1k_2\beta}{k_1+k_2}\sinh\left(\frac{\alpha}{3\sqrt{2}}\right)\bar{p}_1 \tag{40}$$

where $\bar{p}$ is the axial effective stress on the model and $\bar{p}_1$ is the axial effective stress on the flow component.

If we write (40) in the form of finite differences we have

$$\frac{\Delta\bar{p}_1}{\Delta t}=\frac{k_1}{k_1+k_2}\frac{\Delta\bar{p}}{\Delta t}-G\beta\sinh\left(\frac{\alpha}{3\sqrt{2}}\right)\bar{p}_1 \tag{41}$$

where

$$G=\frac{3\sqrt{2}\,k_1k_2}{k_1+k_2}$$

The initial condition for this case is $\bar{p}_1=0$ at $t=0$. For these conditions eq. (41) becomes

$$\frac{\Delta\bar{p}_1}{\Delta t}=\frac{k_1}{k_1+k_2}\quad\frac{\Delta\bar{p}}{\Delta t} \tag{42}$$

which is valid as the limit when $\Delta t\to 0$

or

$$\lim_{\Delta t\to 0}\left[\frac{\Delta\bar{p}_1}{\Delta t}=\frac{k_1}{k_1+k_2}\quad\frac{\Delta\bar{p}}{\Delta t}\right]_{t=0} \tag{43}$$

If we approximate (43) by limiting t to small values we have eq. (42)

or

$$\frac{\Delta\bar{p}_1}{\Delta\bar{p}}=\frac{k_1}{k_1+k_2} \tag{44}$$

Using eq. (21) and (22) we rewrite eq. (1) as

$$\epsilon_1=\frac{1}{4k_2}\quad(\bar{p}-\bar{p}_1) \tag{45}$$

From eq. (30) and (25) we have

$$U^* = \frac{\epsilon_1}{(\epsilon_1)_\infty} \quad (30) \qquad (\epsilon_1)_\infty = \frac{p_o}{4k_2} \quad (25)$$

Combining (25) and (45) with (30) we have

$$U^* = \frac{\bar{p}}{p_o} - \frac{\bar{p}_1}{p_o} = \frac{\bar{p}}{p_o}\left(1 - \frac{\bar{p}_1}{\bar{p}}\right) \tag{46}$$

Differentiating with respect to $\frac{\bar{p}}{p_o}$ gives us

$$\frac{dU^*}{d\left(\frac{\bar{p}}{p_o}\right)} = 1 - \frac{d\bar{p}_1 \Big/ d\left(\frac{\bar{p}}{p_o}\right)}{d\bar{p} \Big/ d\left(\frac{\bar{p}}{p_o}\right)} = \left[1 - \frac{d\bar{p}_1}{d\bar{p}}\right] \tag{47}$$

If we write this in difference form it becomes

$$\frac{\Delta U^*}{\Delta\left(\bar{p}/p_o\right)} = 1 - \frac{\Delta \bar{p}_1}{\Delta \bar{p}} \tag{48}$$

which becomes upon substituting (44)

$$\frac{\Delta U^*}{\Delta \bar{p}/p_o} = 1 - \frac{k_1}{k_1+k_2} = \frac{k_2}{k_1+k_2} \tag{49}$$

We know that the variation of $\bar{p}/p_o$ for $0 < t < tp$ follows the curve obtained by Terzaghi for one dimensional consolidation. Therefore with the coefficient of consolidation, C_v, known from the test data, we can plot a curve of $\bar{p}/p_o$ vs. t.

The experimental data has already been plotted in the form of U* vs. t. Therefore if we can take several small increments of Δt and plot $\Delta U^* / \Delta(\bar{p}/p_o)$ vs. t, the intercept of this curve with $t=0$ gives us the value of the ratio $k_2/(k_1+k_2)$.

Note that with the values of k_1 and k_2 we can evaluate α and $\alpha\beta$ by eq. (29).

The time-deformation curve for the model for $t < tp$ can be calculated in the following manner.

We have written the general differential equation for $\bar{p}_1$ and $\bar{p}$ in terms of finite differences (eq. 40) and have given initial conditions governing its behavior ($\bar{p}_1 = 0$ at $t = 0$). Making use of Euler's method of numerical integration (see for instance Hildebrand, "Introduction to Numerical Analysis") we can get an approximation of the solution of this equation for $\bar{p}_1$.

With the solution of eq. (40) for $\bar{p}_1$ we make use of eq. (46) to relate $\bar{p}_1$ to U*.

$$U^* = \frac{\bar{p}}{p_o} - \frac{\bar{p}_1}{p_o} \tag{46}$$

We can now plot a theoretical curve for the deformation of our model for $t < tp$. In fact this solution can be extended over the entire range of t if desired. However it is cumbersome to apply and its use is not warranted as we already have a convenient solution for $t > tp$ in eq. (28).

All the model parameters have now been determined and a step by step procedure for calculating k_1, k_2, α and β is given as follows. For a complete set of sample calculations see Appendix D.

1 - Plot test data as $U^* = U/U_\infty$ vs. t.

2 - Evaluate $(\epsilon_1)_\infty$ and get k_2 from eq. (25).

3 - Determine C_v from experimental time-deformation curve and plot $\bar{p}/p_o$ vs. t.

4 - Evaluate $k_2/(k_1 + k_2)$ from eq. (49) and consequently k_1 .

5 - Calculate m* and m**, then determine the value of A (figure 5) which best fits m**.

6 - Calculate $\alpha\beta$ by eqs. (29) and (39) .

7 - Use eq. (29) to calculate α and β .

CHAPTER V

TEST RESULTS

1. Comparison of Theoretical Curves with Test Data

In the previous section steps are given for calculating the model parameters k_1, k_2, α, and β. Having these parameters along with the value of A, C_v and $Z(t)/t$, we can construct a curve of U* vs. t and compare it with the experimental curve.

The construction is carried out in two steps corresponding to the two cases given for the model deformation, however the finate difference solution used in case I would be extended over the whole test range. This process is cumbersome and not necessary.

For $t < tp$ we use Euler's method of numerical integration to find the variation of $\bar{p}_1 / p_o$ with time and then calculate U* by eq. (46).

The portion of the curve for $t > tp$ can be gotten with the aid of eq. (28) and figure 4. U_i is computed by eq. (31a). A solution of eq. (28) from figure 4 can be plotted for known values of $Z(t)/t$, A and the ratio of m**/m*. Of course we only use the part of the curve for $t > tp$. Figure 6 gives a graphical picture of these solutions.

Figures 7, 8, 9 and 10 give graphical comparisons of the actual and computed results. It is seen that in each case the agreement of the predicted curves and the experimental data is very good over the entire test range. The curves shown are typical of several types of consolidation curves.

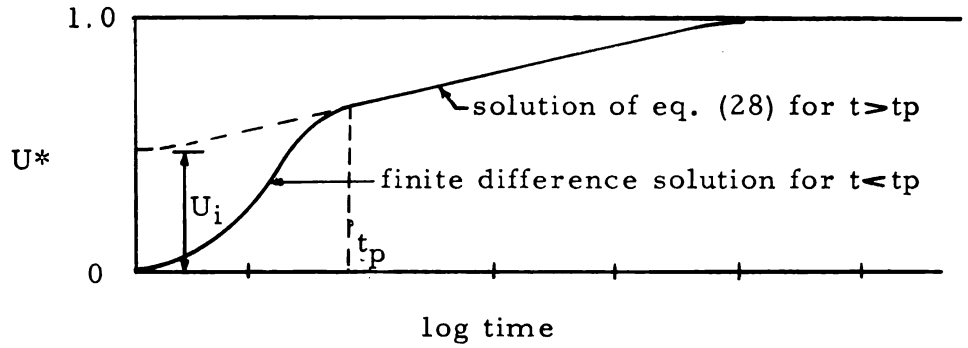

Figure 6. Construction of U* vs. t Curves

Classically, clay consolidation is considered to take place in two stages; the primary consolidation results from drainage under excess hydrostatic pore water pressure, while the secondary consolidation occurs as a result of a rearrangement of clay particles under stress until a stable clay structure is attained. It is obvious that these two effects are not independent, for the clay particles may begin their process of adjustment (flow) long before the drainage has ended.

The solution presented in this thesis accounts for such an overlap. The secondary phase of consolidation is represented by the viscous flow of the dashpot and is expressed in terms of the parameter β. This non-linear element contributes to the deformation of the model over the whole range of stress application. In many cases appreciable amounts of viscous flow takes place shortly after the pressure increment p_o is applied. This results in the common linear relationship of U* vs. log t (as observed for the Sault Ste. Marie and Marine City clays).

The secondary consolidation of the Mexico City clays differs considerably from those described above. As shown by Girault (1960), the unusual shape of these deformation curves occurs for small loading increments ($\frac{\Delta p}{p} \ll 1$). In such cases we see that even after primary consolidation

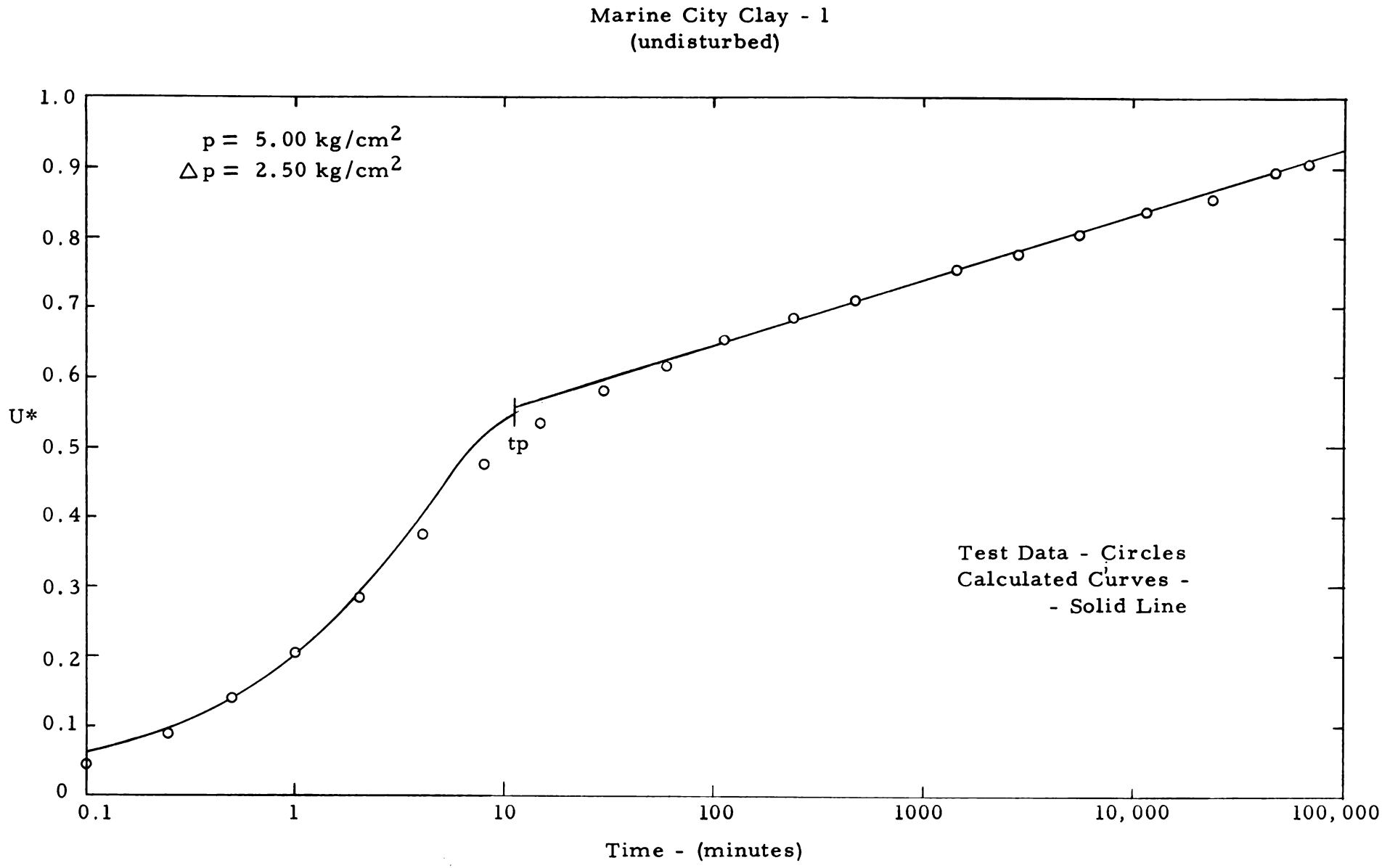

Figure 7. Experimental vs. Theoretical Curves - 1

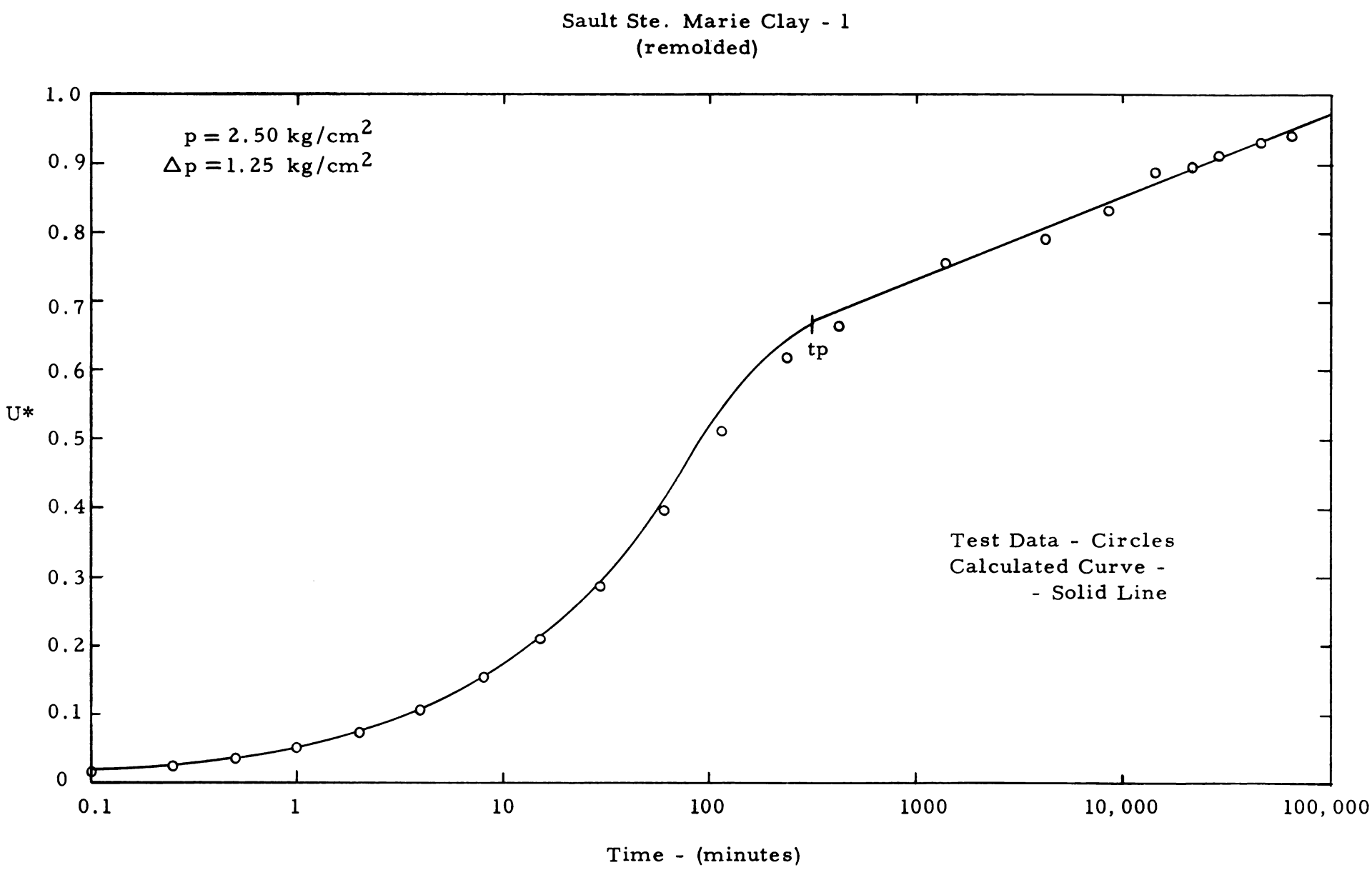

Figure 8. Experimental vs. Theoretical Curves - 2

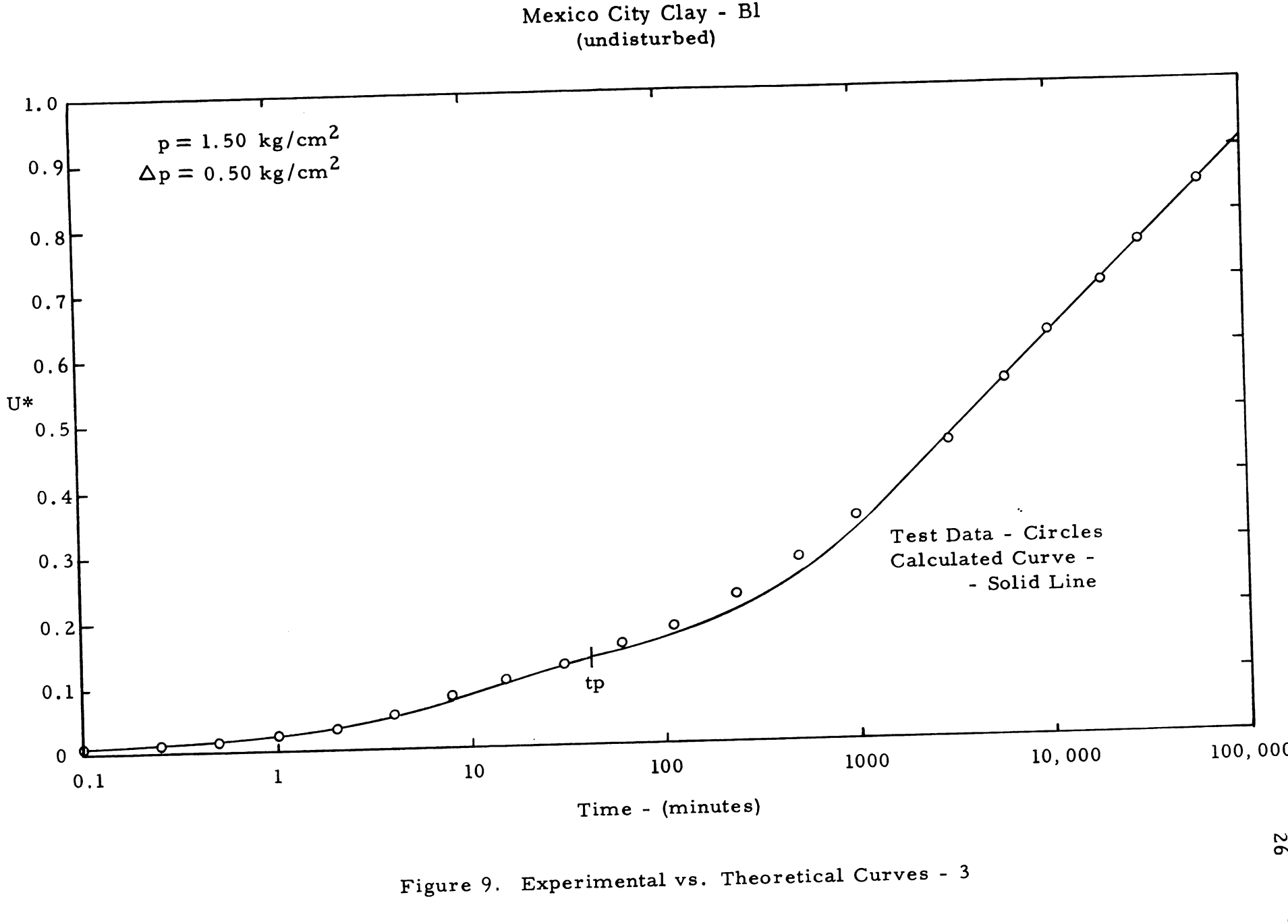

Figure 9. Experimental vs. Theoretical Curves - 3

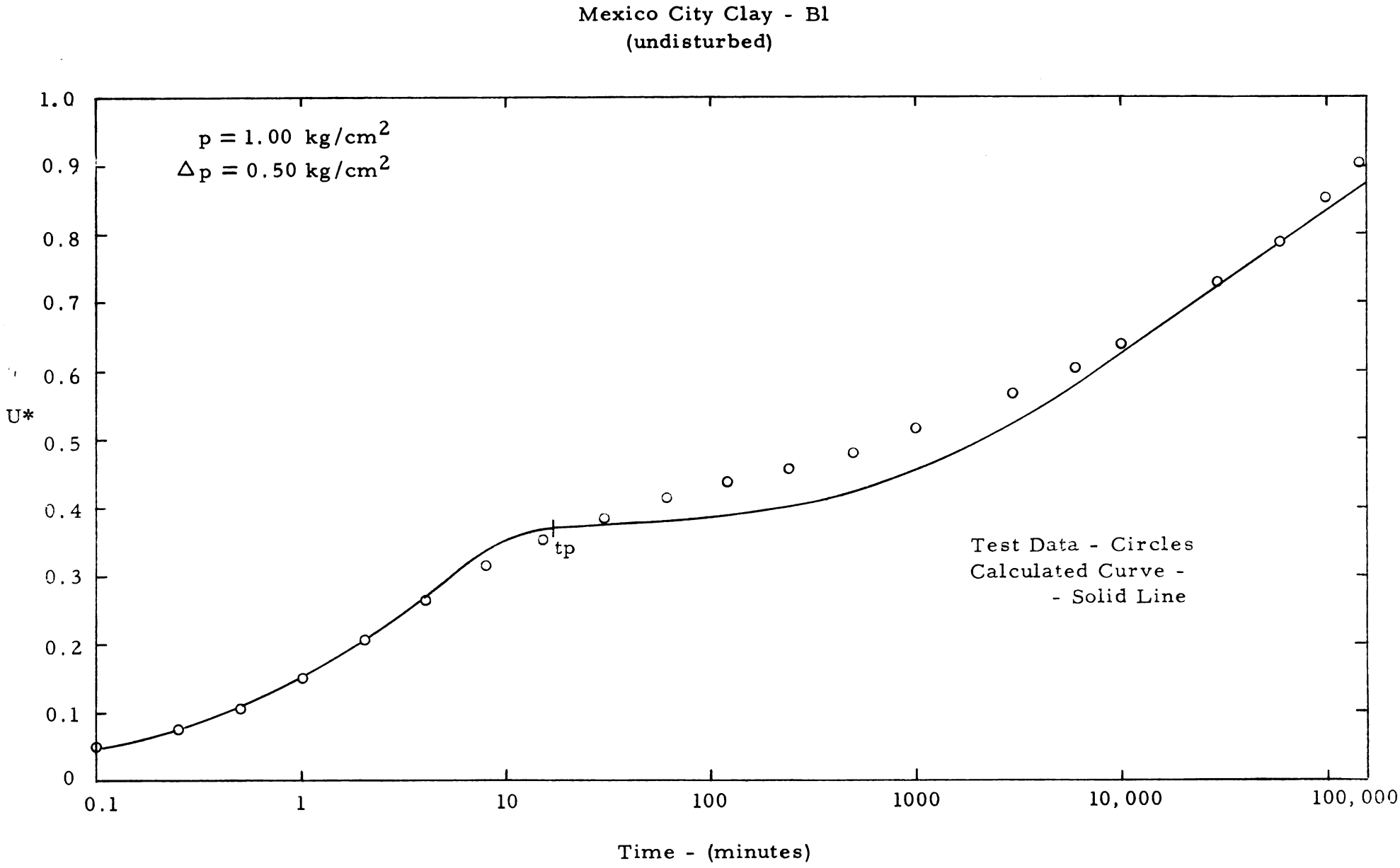

Figure 10. Experimental vs. Theoretical Curves - 4

has been completed, the viscous flow of the particles is still very small and in some cases negligible. However most of the viscous flow occurs after t_p and very large secondary consolidation may take place before an equilibrium is reached. Our model is still able to reproduce faithfully the experimental data.

2. Variation of Model Parameters

As there is good agreement between theoretical and experimental data, we now look at the model parameters individually and study their variation with the loading conditions. A summary of the calculated parameters is given in Appendix C, while the variation of $k_1/(k_1+k_2)$, α and β with stress is shown graphically in Appendix D.

The spring constants k_1 and k_2 represent the elastic response of the clay structure while k_2 represents the effect of stress on non-flowing (elastic) contacts. In the remolded samples of Marine City and Sault Ste. Marie clays, k_2 remains fairly constant at low stress levels but increases at high stresses. On the undisturbed samples of the same clay, it again remains constant at low stresses but increases rapidly at stresses that exceed the preconsolidation pressure, p_c. In the undisturbed Mexico City clays, k_2 decreases with increasing stress until the preconsolidation pressure is reached after which it increases markedly.

The increase in k_2 at stresses exceeding p_c is what we would expect because in this stress range the clay is compressed to progressively smaller void ratios. Consequently the structure becomes more rigid and the elastic bonds are able to carry larger stresses.

The ratio of $k_1/(k_1+k_2)$ represents the portion of the applied stress that acts on the flowing contacts. We would expect that, for undisturbed samples, at high stress levels more contacts are broken and flow. This should result in an increasing trend in the ratio of $k_1/(k_1+k_2)$.

Such a prediction agrees with the data shown in Appendix B.

In all cases except one, the undisturbed samples showed increases in $k_1/(k_1+k_2)$ with increasing stress. Figures 11 and 12 show variation of $k_1/(k_1+k_2)$ as well as α and β with increasing stress for two samples.

For the remolded clays, the ratio varies little over the entire stress range and has a low value. This indicates that under each new load increment the stress on the flowing bonds is a constant proportion of the total stress.

The parameter α, as defined by rate process theory, is an indicator of interparticle movements. It is directly proportional to λ, the average distance between bonds (or the average "jump" distance) and inversely proportional to the number of flowing contacts, ν.

As the total stress increases, the stress on the flowing contacts increases; we would expect the number of flowing contacts and flowing bonds to increase directly with the stress.

The data shows that for all tests α decreases with increasing stress as we predicted it should.

It might be noted that α would also decrease if λ decreased at high stresses, however λ represents an average value of all jump distances and is unlikely to decrease significantly.

The parameter β also represents viscous movement of bonds and is defined as

$$\beta = 2\frac{\lambda}{\lambda_1}\frac{kt}{h} \exp(-\Delta F/RT)$$

where λ_1 is the distance between planes of slip and ΔF represents the activation energy required to initiate bond "jumps".

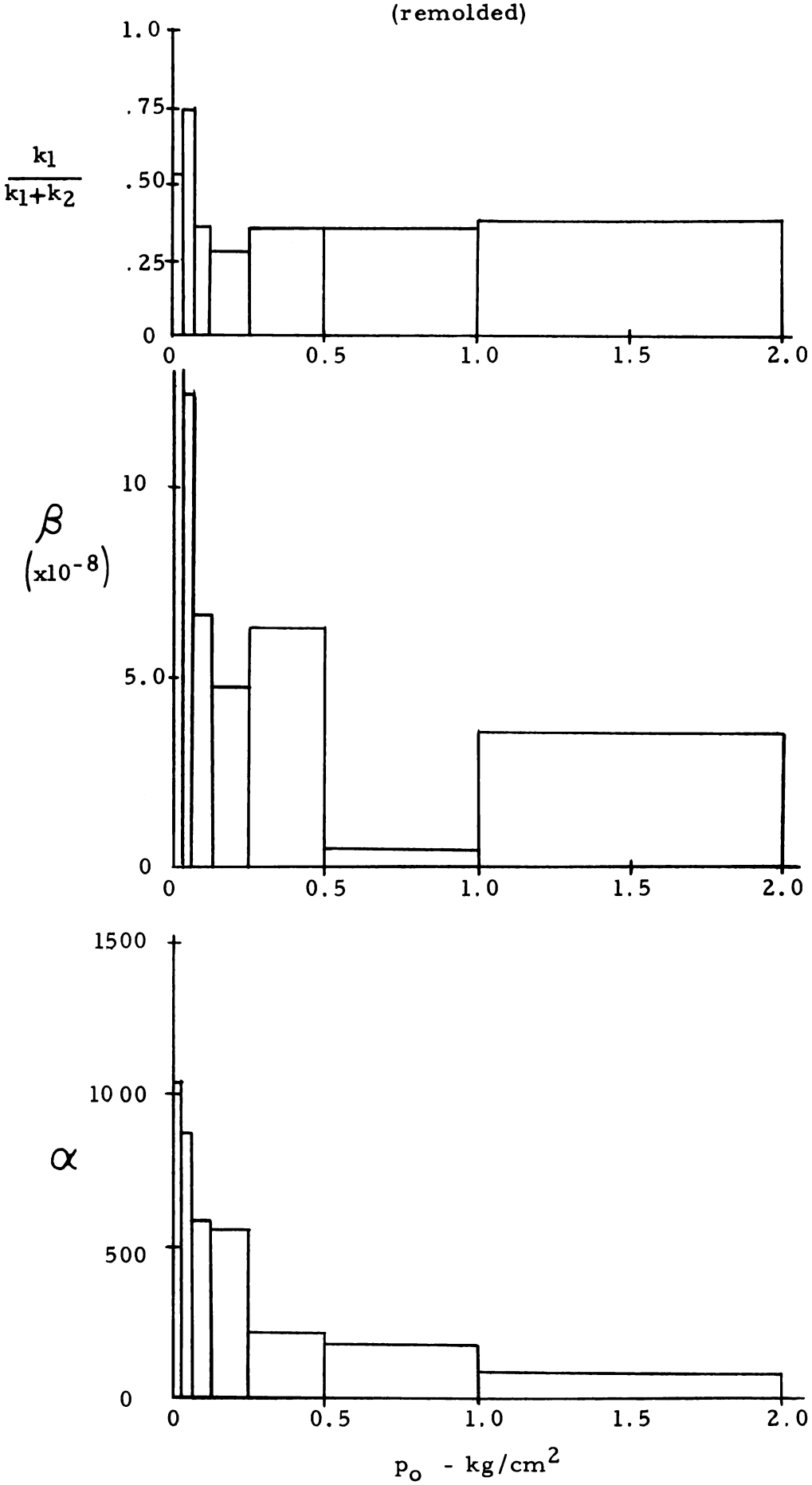

Figure 11. Variation of Model Parameters with Stress

Mexico City Clay - B5
(undisturbed)

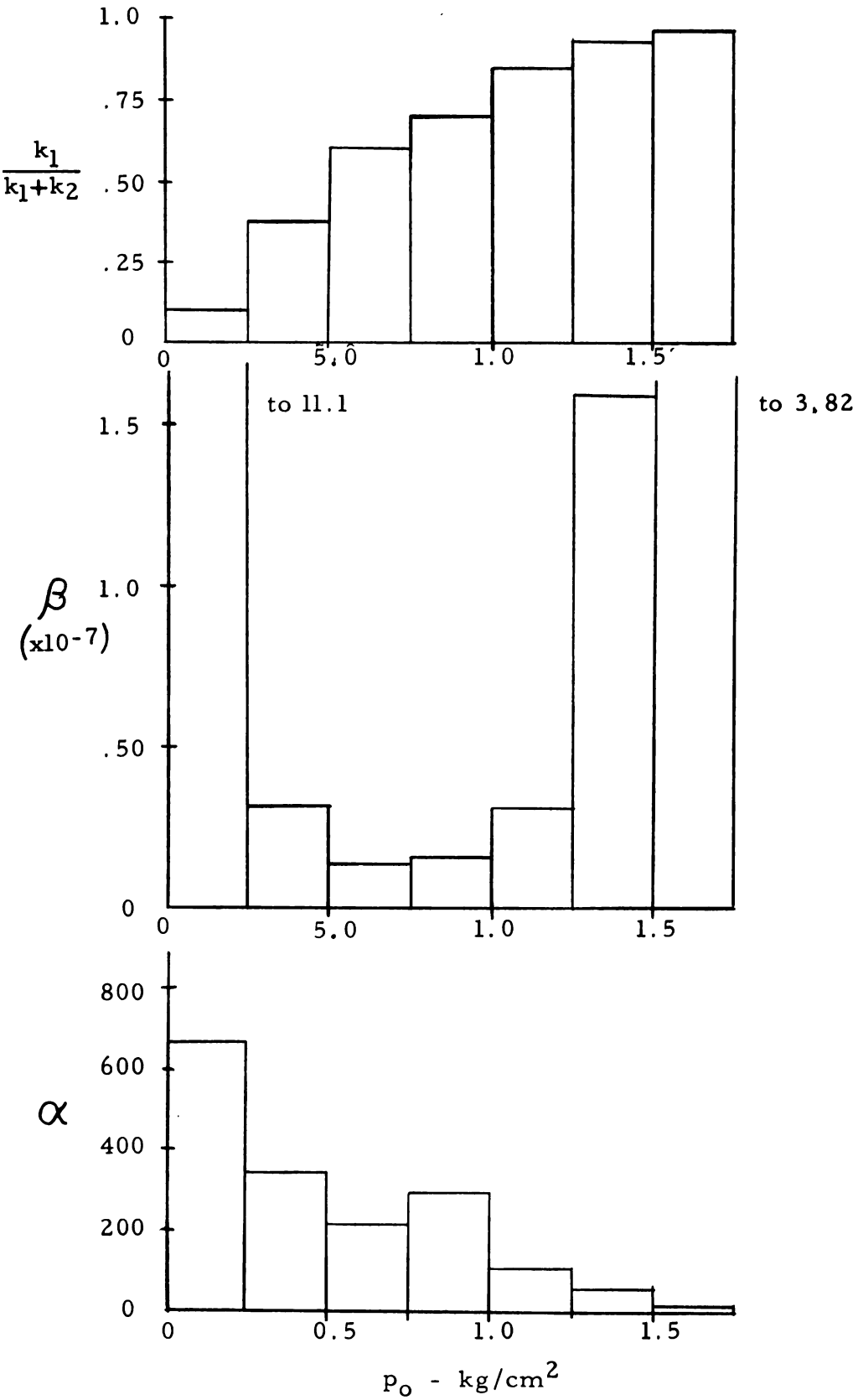

Figure 12. Variation of Model Parameters with Stress

If the ratio of $\frac{\lambda}{\lambda_1}$ remains constant over the entire stress range β would depend only on the activation energy. In this case we would expect β to decrease with increasing stress, for at high stresses the bonds with low strengths have been broken and those remaining have progressively higher strength and greater activation energy.

In a consolidation test, however, the strains are essentially in one direction. Final strains can approach 10 to 12% of the original height of the sample which could bring about a decrease in λ_1, the distance between the planes of slip.

A decrease in λ_1 would increase the ratio of $\frac{\lambda}{\lambda_1}$ and would cause an increase in β.

The undisturbed and remolded Marine City clays have high intial β values which generally decrease with increasing stress, indicating a constant increase in ΔF.

However, from the data we see that the Mexico City clays have an initially large value of β which decreases with increasing stress but increases rapidly at stress levels around the preconsolidation pressure. Such behavior is also present in the remolded Sault Ste. Marie clay. It would be well to note here that both of these clays have very high initial void ratios.

The decrease in β for low stresses in the above clays can be explained by an increase in ΔF. As the preconsolidation pressure is reached, however, large compressions and large structural changes take place under additional stresses. This would suggest that λ may increase, as the average jumps would be longer, and λ_1 decreases due to large compression in the axial direction. Both of these factors would increase β. At stresses beyond p_c it is probable that β will again decrease because ΔF will steadily increase.

CHAPTER VI

CONCLUSION

The analysis in the previous section indicates that the model adequately describes the deformational characteristics of a variety of clays. It has been shown that there is good agreement between the calculated curves and the experimental data.

The main factors governing the shape of the curves produced by our deforming model are the slope constant, A, the ratio of $k_1/(k_1+k_2)$, the coefficient of compressibility, C_v, and the ratio of $Z(t)/t$. A further look tells us that the value we pick for A depends on the ratio of $m^*/\bar{m}$ which in turn is a function of $k_1/(k_1+k_2)$. By combining these factors in various proportions we can duplicate a number of typical deformation curves for clays.

Figure 13 shows two different systems for classifying types of consolidation curves; one by K. Y. Lo (1961) and the other by G. A. Leonards (1961). Girault (1960) applied Leonard's classification to Mexico City clay and showed their relation to the loading ratio used in testing.

We have already shown that these curves can be duplicated with the model of figure 1. To duplicate curves of Type (I) requires that we have a small $k_1/(k_1+k_2)$ ratio, a fairly small value for C_v and a large ratio of $Z(t)/t$.

Lo's type II curve is merely an extension of Type I and can be produced with a value of $k_1/(k_1+k_2)$ between 0.3 and 0.6, a fairly small value of C_v and a large ratio of $Z(t)/t$.

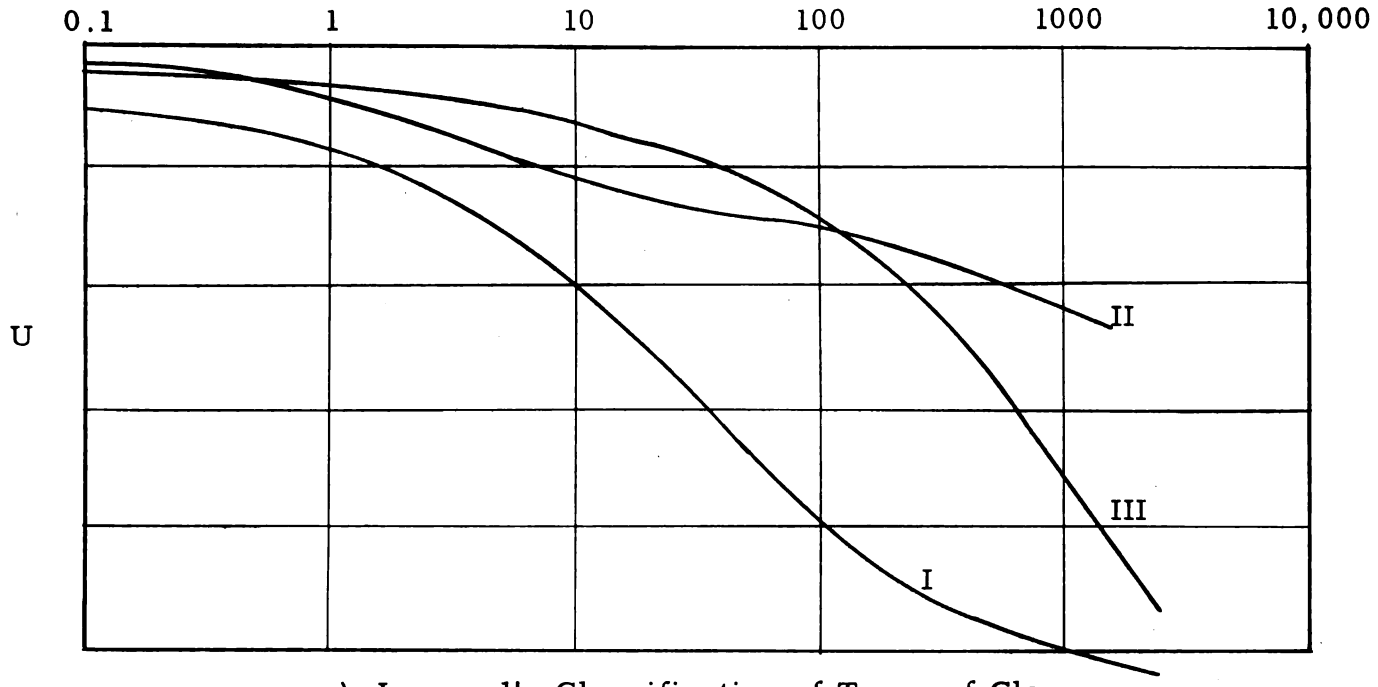

a) Leonard's Classification of Types of Clay Deformation Curves

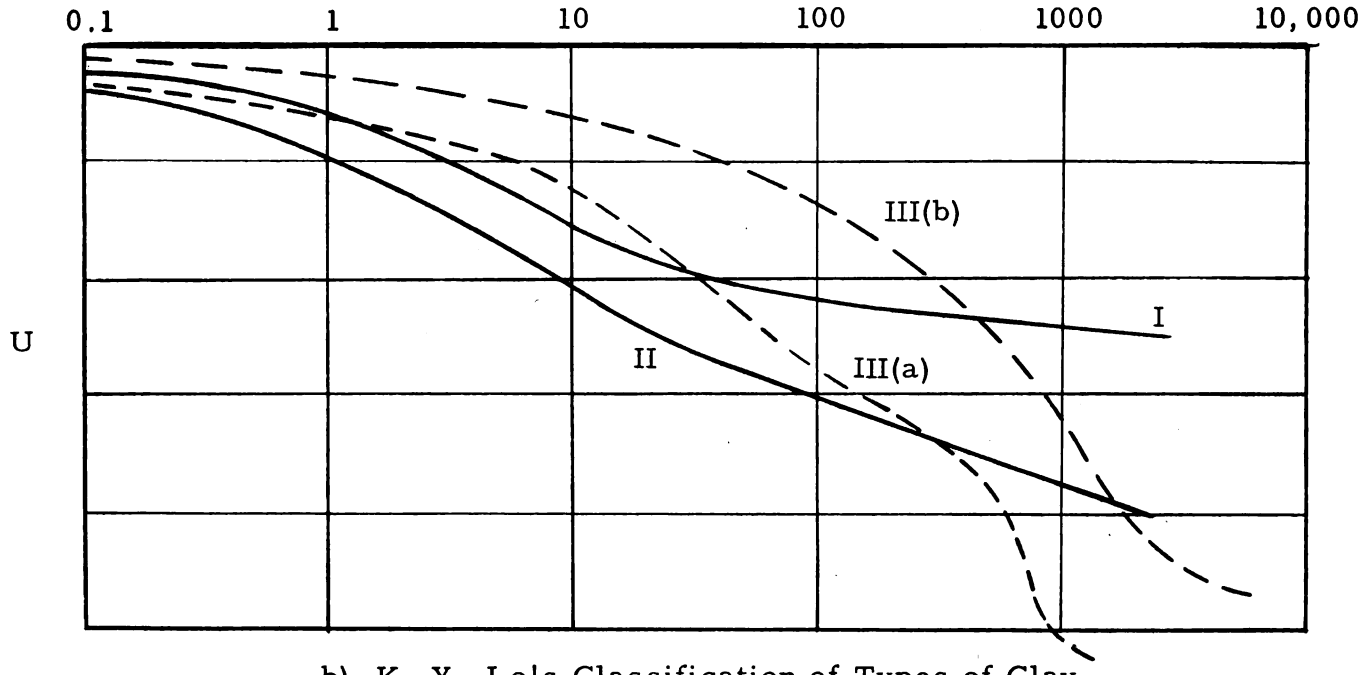

b) K. Y. Lo's Classification of Types of Clay Deformation Curves

Figure 13. Classification of Clay Deformation Curves

Similarly, Leonard's Type II curve can be duplicated with a value of $k1/(k_1 + k_2)$ around 0.15.

Lo's Type III(b) curve is similar to Leonard's Type III curve and neither shows any primary stage. A curve of this type can be approximated by using a very large value of $k_1/(k_1 + k_2)$, a large value for C_v and a small ratio of $Z(t)/t$. Curves of this type occur most frequently in very compressible clays subjected to equal loading increments as can be seen from the tests on Mexico City clay.

Thus we conclude that the proposed model represents an effective way of representing the consolidation characteristics of a wide range of clay types, including both remolded and undisturbed samples.

The fact that the calculated curves compare very well with the actual deformation data indicates that this is also an effective way to calculate the rheological parameters of the model. These have been shown to behave consistently with the material parameters as proposed by the rate-theory analysis. The variation of these material parameters gives us an important insight into the mechanics of clay deformation.

The rheological model also gives us a solution for the entire consolidation process, which would seem to be more convenient and reasonable than an arbitrary separation of the phenomenon into primary and secondary stages. Also, while the model gives good agreement with a wide variety of deformation curves, it is itself simple and the equations governing its behavior offer relatively simple solutions.

BIBLIOGRAPHY

Bishop, A. W., "Test Requirements for Measuring the Coefficient of Earth Pressure at Rest," Brussels Conference on Earth Pressure Problems, Vol. 1, 1958, pp. 2-14.

Christensen and Wu, "Analysis of Clay Deformation as a Rate Process," Journal of the Soil Mechanics and Foundations Division, ASCE, Vol. 90, No. SM6, Nov., 1964, pp. 125-157.

Eyring, H. and Halsey, G., "The Mechanical Properties of Textiles - The Simple Non-Newtonian Model," High Polymer Physics - A Symposium, 1948, pp. 61-116.

Gibson, R. E. and Lo, K. Y., "A Theory of Consolidation for Soils Exhibiting Secondary Compression," Norwegian Geotechnical Institute Publication No. 41, (also Acta Polytechnica Scandinavia, 296/191, Ci 10), 1961

Girault, Pablo, "A Study on the Consolidation of Mexico City Clay," Ph.D. Thesis, Purdue University, 1960.

Glasstone, S., Laidler, K., and Eyring, H.,"The Theory of Rate Processes," McGraw-Hill Publishing Company, Inc., New York, New York, 1941.

Hildebrand, F. B., "Introduction to Numerical Analysis," McGraw-Hill New York, New York, 1956.

Leonards, G. A. and Altschaffel, A. G., "Compressibility of a Clay," Journal of the Soil Mechanics and Foundations Division, ASCE, Vol. 90, No. SM5, Sept. 1964, pp. 133-155.

Leonards, G. A. and Girault, P., "A Study of the One-Dimensional Consolidation Test," Proceedings of the Fifth International Conference on Soil Mechanics and Foundation Engineering, Vol. 1, Paris, 1961, pp. 213-224.

Lo, K. Y., "Secondary Compression of Clays," Journal of the Soil Mechanics and Foundations Division, ASCE, Vol. 87, No. SM4, August, 1961, pp. 61-87.

Mitchel, J. K., "Shearing Resistance of Soils as a Rate Process," Journal of the Soil Mechanics and Foundations Division, ASCE, Vol. 90, SM4, 1964.

Murayama and Shibata, "Flow and Stress Relaxation of Clays," Rheology and Soil Mechanics Symposium of the International Union of Theoretical and Applied Mechanics, April, 1964.

Rosenquist, I. Th., "Physical-Chemical Properties of Soils: Soil-Water Systems," Journal of the Soil Mechanics and Foundations Division, ASCE, Vol. 85, No. SM2, Proc. Paper 2000, April, 1959, pp. 31-53.

Schiffmann, R. L., Ladd, C. C., Chen, A. T-F., "The Secondary Consolidation of Clay," Symposium on Rheology and Soil Mechanics of the International Union of Theoretical and Applied Mechanics, April, 1964.

Tan, T. K., (Discussion), Proceedings of the Third International Conference on Soil Mechanics and Foundation Engineering, Vol. 3, 1953, p. 129.

Terzaghi, K. and Peck, R. B., "Soil Mechanics in Engineering Practice," John Wiley and Sons, Inc., New York, New York, 1948.

Zeevaert, L., "Consolidation of Mexico City Volcanic Clay," ASTM, Spec. Tech. Pub. 232, 1957, pp. 18-32.

APPENDIX A

TEST DATA - TABULAR FORM

TEST DATA

1. Clay - Marine City (undisturbed)
   Sample 1

Load Inc. (kg/cm^2)	Duration of Test (days)	C_v (in^2/min)	A	$\alpha\beta_1$ ($\times10^{-5}$)	$\alpha\beta_2$ ($\times10^{-5}$)
0 - 0.625	5	3.38×10^{-2}	5.30	2.66	8.20
0.625 - 1.25	5	1.77×10^{-2}	7.60	4.26	3.58
1.25 - 2.50	8	2.32×10^{-2}	7.60	5.35	2.77
2.50 - 5.00	234	2.56×10^{-2}	9.90	2.24	0.05
5.00 - 10.00	114	2.44×10^{-2}	9.90	0.075	0.068

2. Clay - Marine City (remolded)
   Sample 2a

Load Inc. (kg/cm^2)	Duration of Test (days)	C_v (in^2/min)	A	$\alpha\beta_1$ ($\times10^{-5}$)	$\alpha\beta_2$ ($\times10^{-5}$)
0 - 0.031	4	3.02×10^{-2}	3.90	156	260
0.031 - 0.0625	8	9.2×10^{-3}	4.60	11.0	10.8
0.0625 - 0.125	53	6.0×10^{-4}	3.90	5.02	3.89
0.125 - 0.250	81	5.0×10^{-4}	4.60	4.10	2.64
0.250 - 0.500	69	8.5×10^{-4}	4.60	0.953	1.37
0.500 - 1.00	139	1.78×10^{-3}	7.60	0.760	0.105
1.00 - 2.00	117	2.6×10^{-3}	7.60	0.726	0.301

3. Clay - Marine City (undisturbed)
   Sample 2b

Load Inc. (kg/cm^2)	Duration of Test (days)	C_v (in^2/min)	A	$\alpha\beta_1$ ($\times10^{-7}$)	$\alpha\beta_2$ ($\times10^{-7}$)
0.500 - 1.00	20	4.25×10^{-2}	5.30	795	885
1.00 - 2.00	48	4.88×10^{-2}	7.60	49.6	52.4
2.00 - 4.00	185	2.92×10^{-2}	9.90	6.56	3.59
4.00 - 8.00	156	1.5×10^{-2}	12.0	7.64	4.96
8.00 - 16.00	253	0.69×10^{-2}	9.90	2.24	1.15

TEST DATA (cont'd)

4. Clay - Sault Ste. Marie (remolded)
Sample 1

Load Inc. (kg/cm^2)	Duration of Test (days)	C_v (in^2/min)	A	$\alpha\beta_1$ ($\times 10^{-6}$)	$\alpha\beta_2$ ($\times 10^{-6}$)
0 - 0.156	6	2.45×10^{-2}	6.20	53.7	33.8
0.312 - 0.625	73	1.36×10^{-3}	4.60	18.8	19.3
0.625 - 1.25	172	$.802\times10^{-3}$	4.60	12.9	11.6
1.25 - 2.50	114	$.982\times10^{-3}$	5.30	5.16	6.78
2.50 - 5.00	27	1.21×10^{-3}	6.20	26.0	8.96

5. Clay - Mexico City (undisturbed)
Sample A5

Load Inc. (kg/cm^2)	Duration of Test (days)	C_v (cm^2/min)	A	$\alpha\beta_1$ ($\times 10^{-5}$)	$\alpha\beta_2$ ($\times 10^{-5}$)
0 - 0.25	4	0.770	4.60	105	147
0.25 - 0.50	40	0.705	9.90	1.06	0.358
0.50 - 1.00	132	0.458	9.90	0.529	0.157
1.00 - 2.00	125	0.0026	3.22	7.64	3.36
2.00 - 4.00	31	0.0108	4.60	100	26.8
4.00 - 8.00	69	0.0078	3.90	5.20	3.13

6. Clay - Mexico City (undisturbed)
Sample B1

Load Inc. (kg/cm^2)	Duration of Test (days)	C_v (cm^2/min)	A	$\alpha\beta_1$ ($\times 10^{-5}$)	$\alpha\beta_2$ ($\times 10^{-5}$)
0 - 0.25	11	0.467	4.60	152	256
0.25 - 0.50	56	0.348	7.60	5.28	1.55
0.50 - 1.00	108	0.167	15.0	0.482	0.106
1.00 - 1.50	90	0.0475	6.20	0.885	1.06
1.50 - 2.00	132	0.128	5.30	1.63	2.29
2.00 - 2.50	180	0.0653	4.60	1.85	0.404

TEST DATA (cont'd)

7. Clay - Mexico City (undisturbed)
Sample B5

Load Inc. (kg/cm^2)	Duration of Test (days)	C_v (cm^2/min)	A	$\alpha\beta_1$ ($\times 10^{-6}$)	$\alpha\beta_2$ ($\times 10^{-6}$)
0 - 0.25	4	0.192	3.90	765	733
0.25 - 0,50	35	0.196	7.60	9.45	10.8
0.50 - 0.75	70	0.115	7.60	3.95	2.76
0.75 - 1.00	167	0.065	12.0	4.55	0.305
1.00 - 1.25	90	0.057	5.30	7.70	3.18
1.25 - 1.50	132	0.047	3.22	9.84	9.45
1.50 - 1.75	183	0.046	1.00	5.34	6.72

8. Clay - Mexico City (undisturbed)
Sample C5

Load Inc. (kg/cm^2)	Duration of Test (days)	C_v (cm^2/min)	A	$\alpha\beta_1$ ($\times 10^{-5}$)	$\alpha\beta_2$ ($\times 10^{-5}$)
0 - 0.25	33	0.625	9.90	7.10	5.85
0.25 - 0.50	70	0.315	5.30	1.59	0.730
0.50 - 1.50	76	0.125	9.90	2.07	5.00
1.50 - 2.50	97	0.185	6.20	2.08	15.2
2.50 - 3.50	57	0.162	3.60	1.17	1.68
3.50 - 4.50	10	0.171	1.00	4.77	2.04

APPENDIX B

EXPERIMENTAL TIME-DEFORMATION CURVES

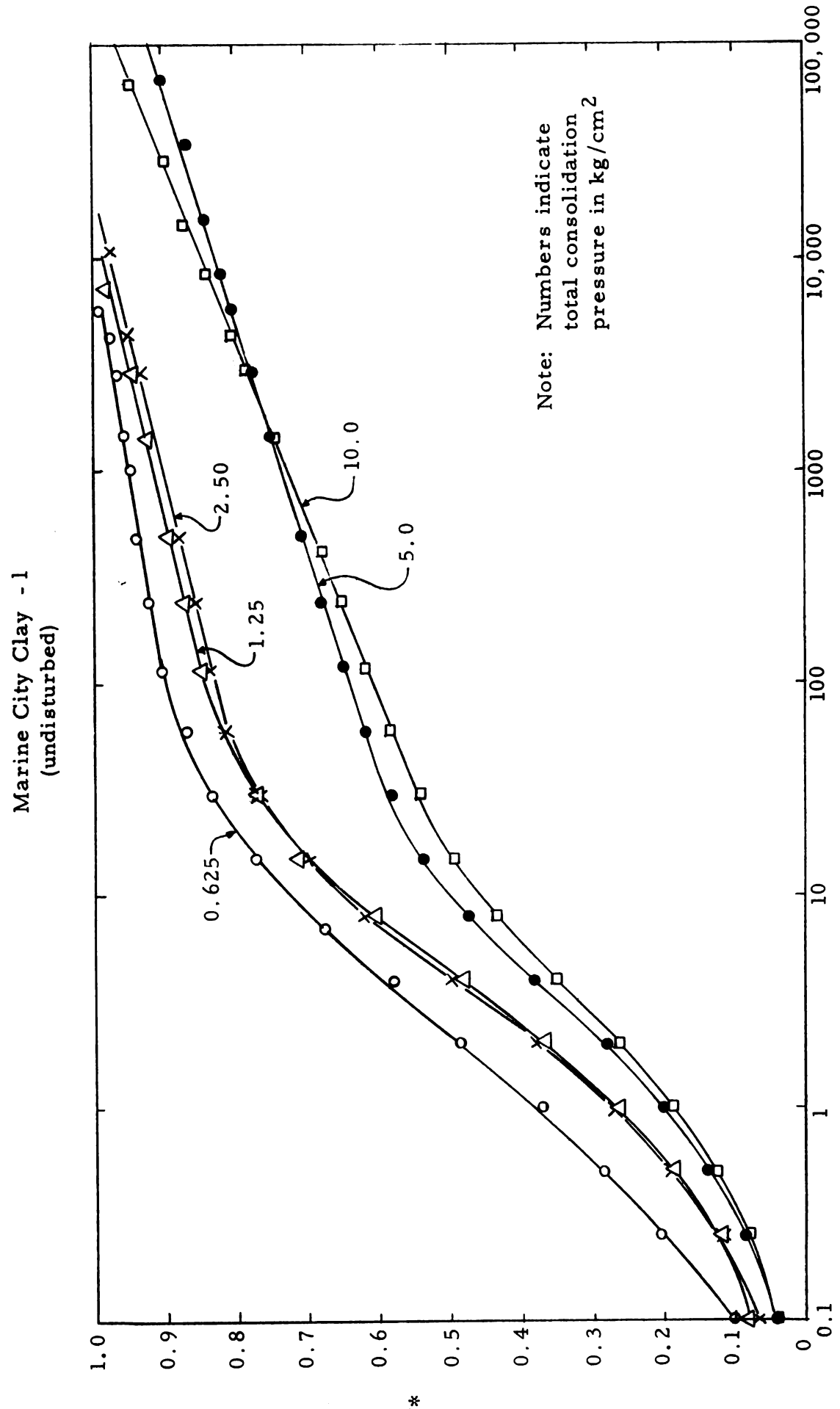
Marine City Clay - 1
(undisturbed)
Note: Numbers indicate
total consolidation
pressure in kg/cm2
0.625
1.25
2.50
5.0
10.0
J*
Time - (minutes)
0
0.1
0.2
0.3
0.4
0.5
0.6
0.7
0.8
0.9
1.0
0.1
1
10
100
1000
10,000
100,000

Marine City Clay - 2a
(remolded)

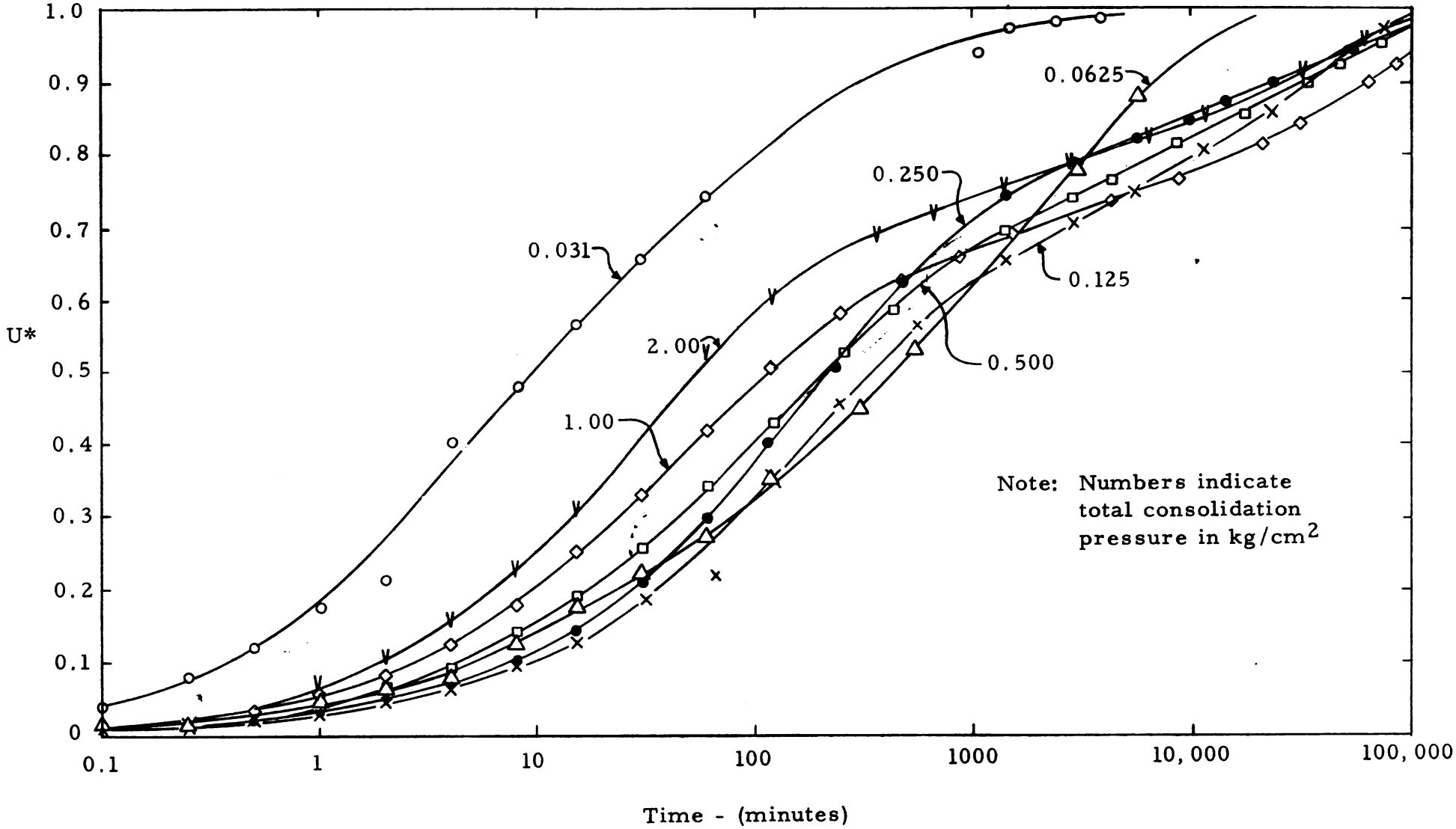

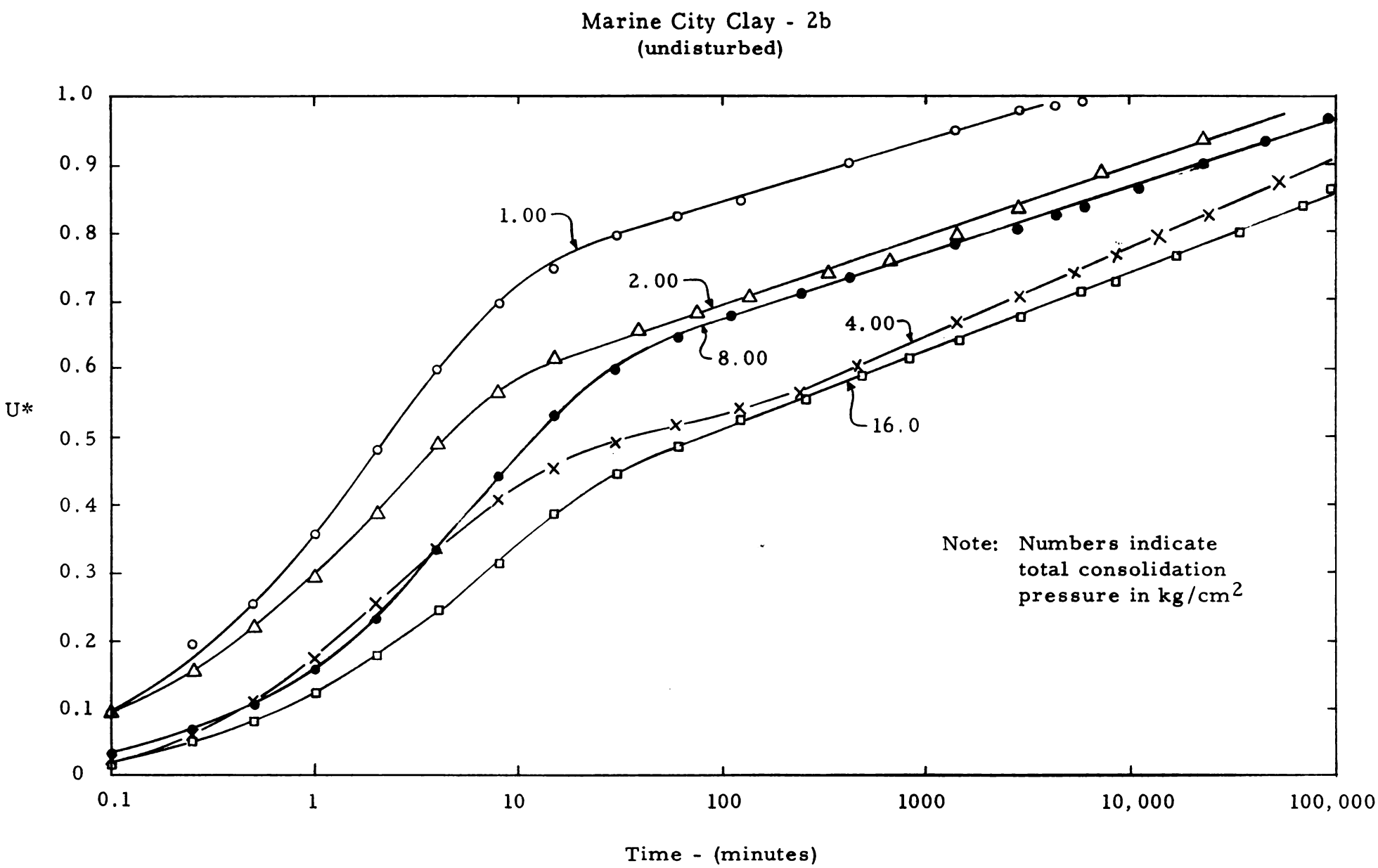
Marine City Clay - 2b
(undisturbed)
1.0
0.9
0.8
0.7
0.6
0.5
0.4
0.3
0.2
0.1
0
U*
1.00
2.00
4.00
8.00
16.0
Note: Numbers indicate total consolidation pressure in kg/cm2
0.1
1
10
100
1000
10,000
100,000
Time - (minutes)

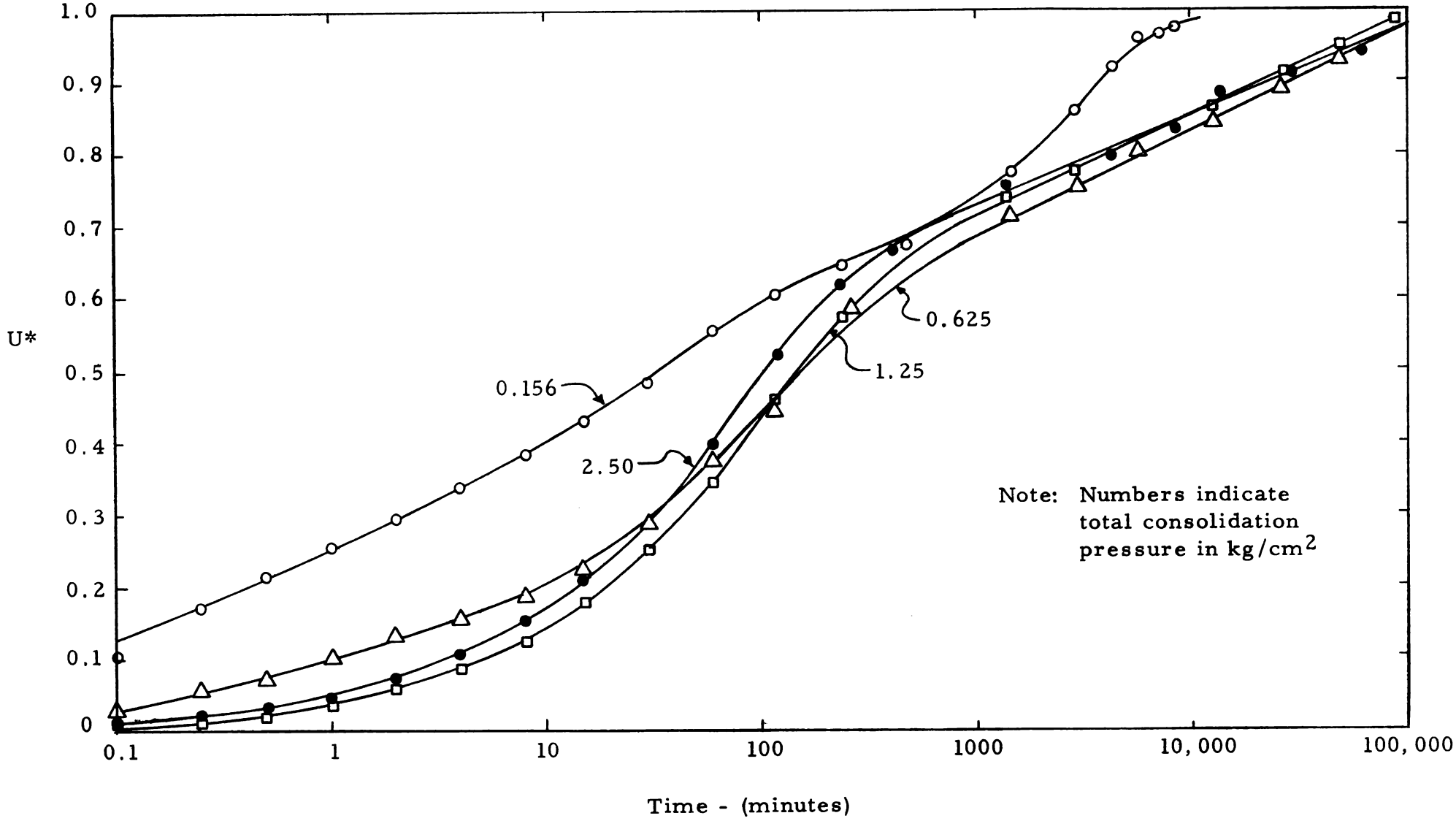
Sault Ste. Marie Clay - 1
(remolded)
1.0
0.9
0.8
0.7
0.6
0.5
0.4
0.3
0.2
0.1
0
U*
0.156
2.50
0.625
1.25
Note: Numbers indicate total consolidation pressure in kg/cm2
0.1
1
10
100
1000
10,000
100,000
Time - (minutes)

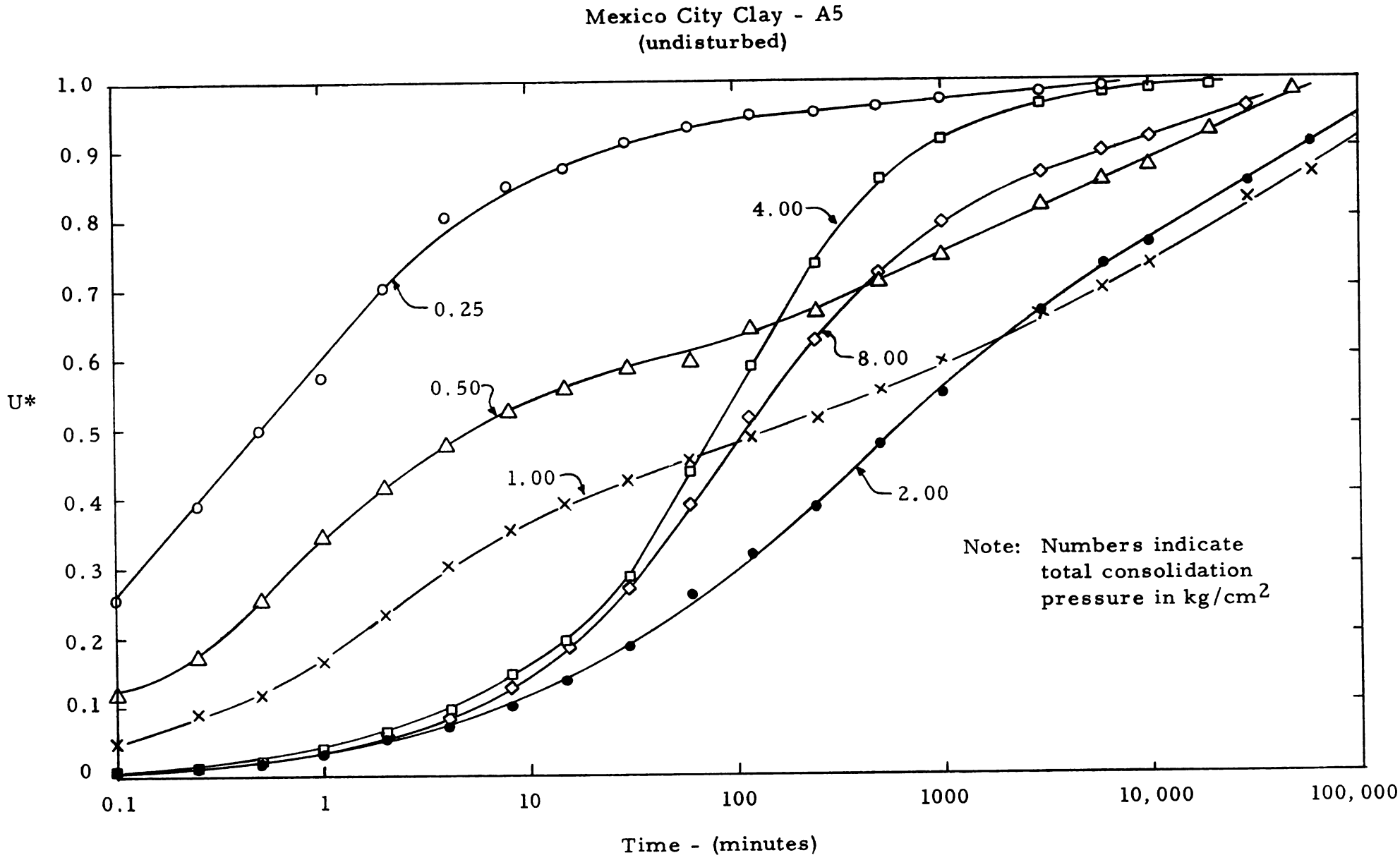
Mexico City Clay - A5
(undisturbed)
1.0
0.9
0.8
0.7
0.6
0.5
0.4
0.3
0.2
0.1
0
U*
0.25
0.50
1.00
2.00
4.00
8.00
Note: Numbers indicate total consolidation pressure in kg/cm2
0.1
1
10
100
1000
10,000
100,000
Time - (minutes)

Mexico City Clay - Bl
(unidsturbed)

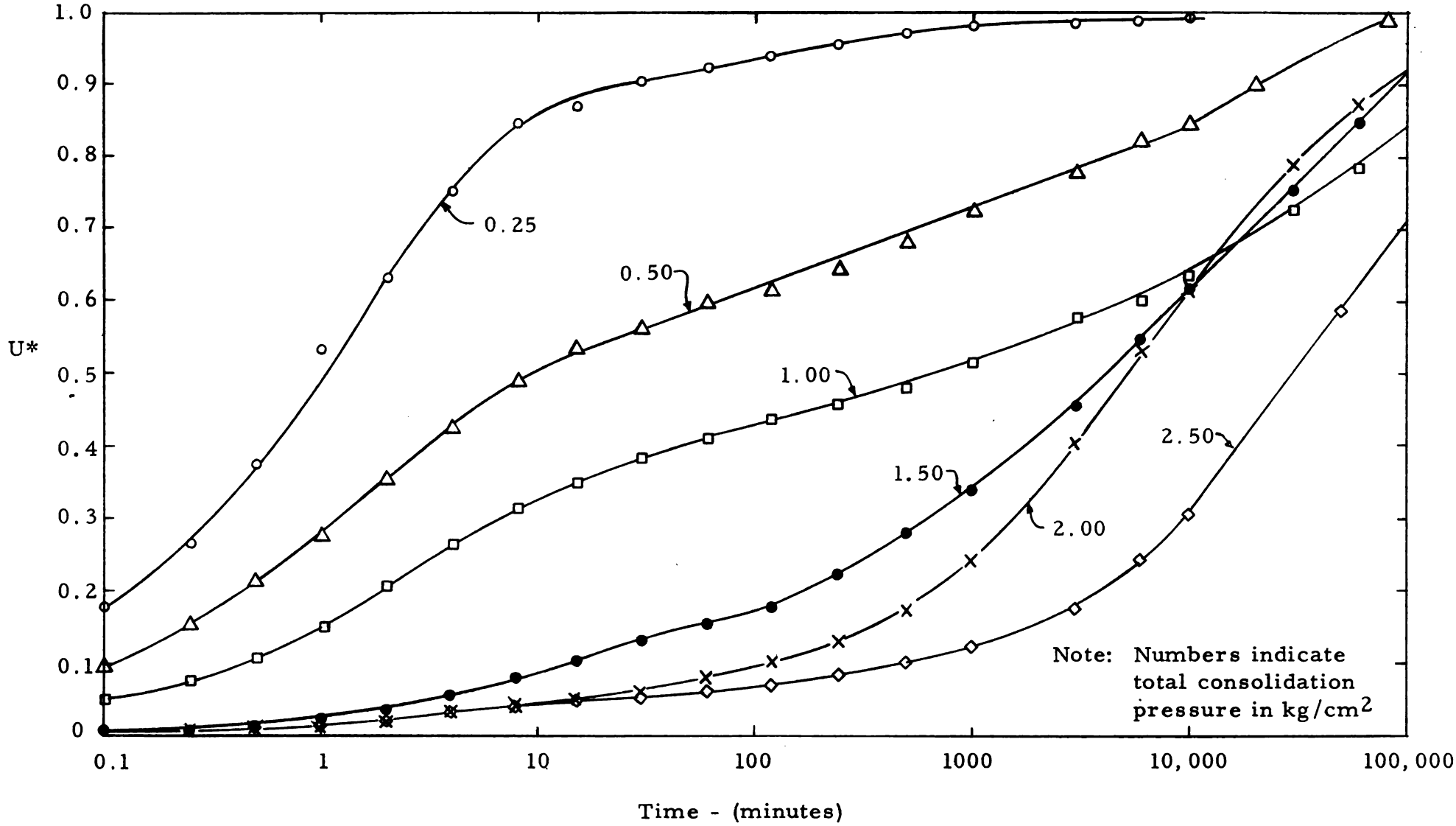

Mexico City Clay - B5
(undisturbed)

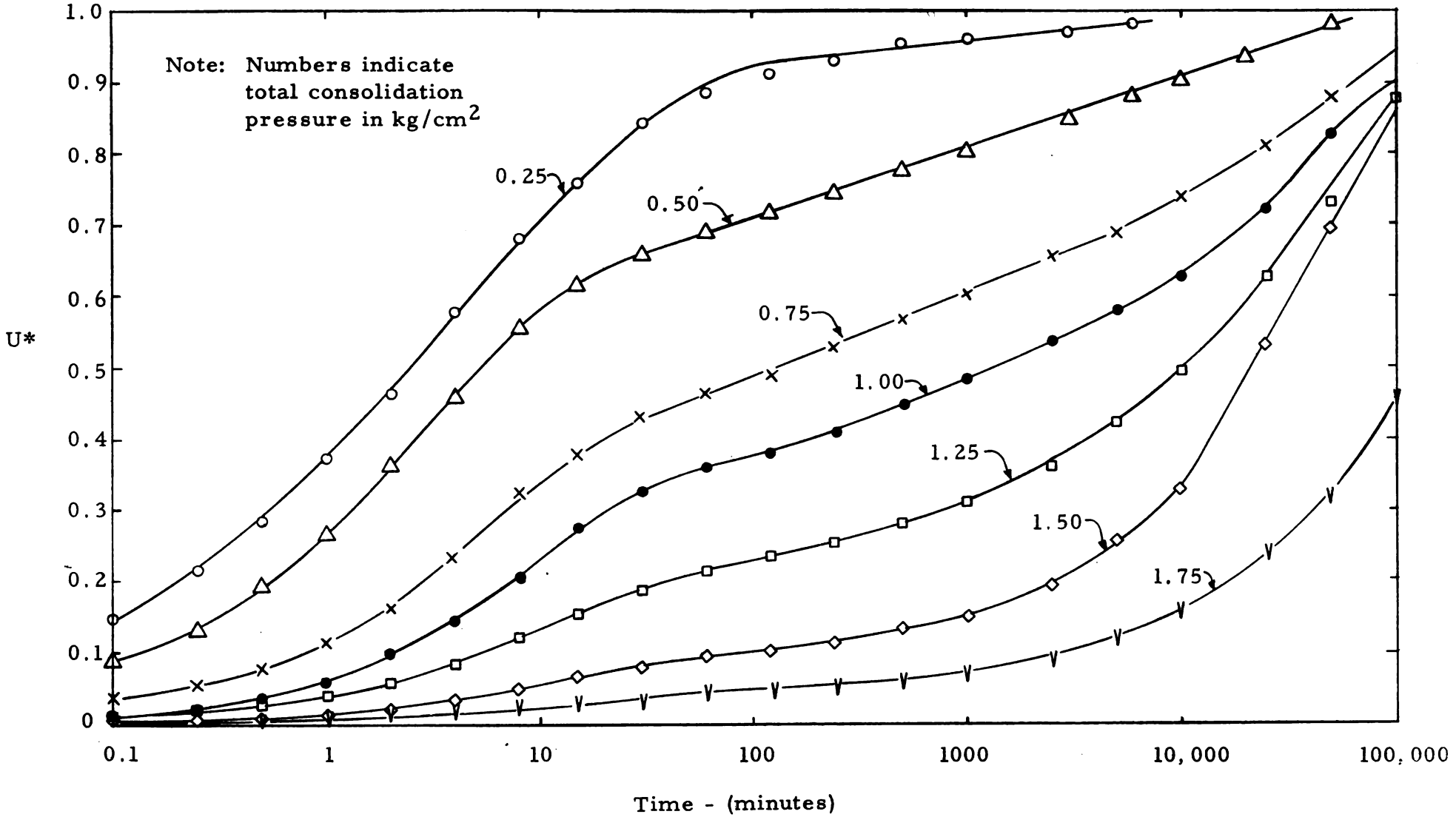

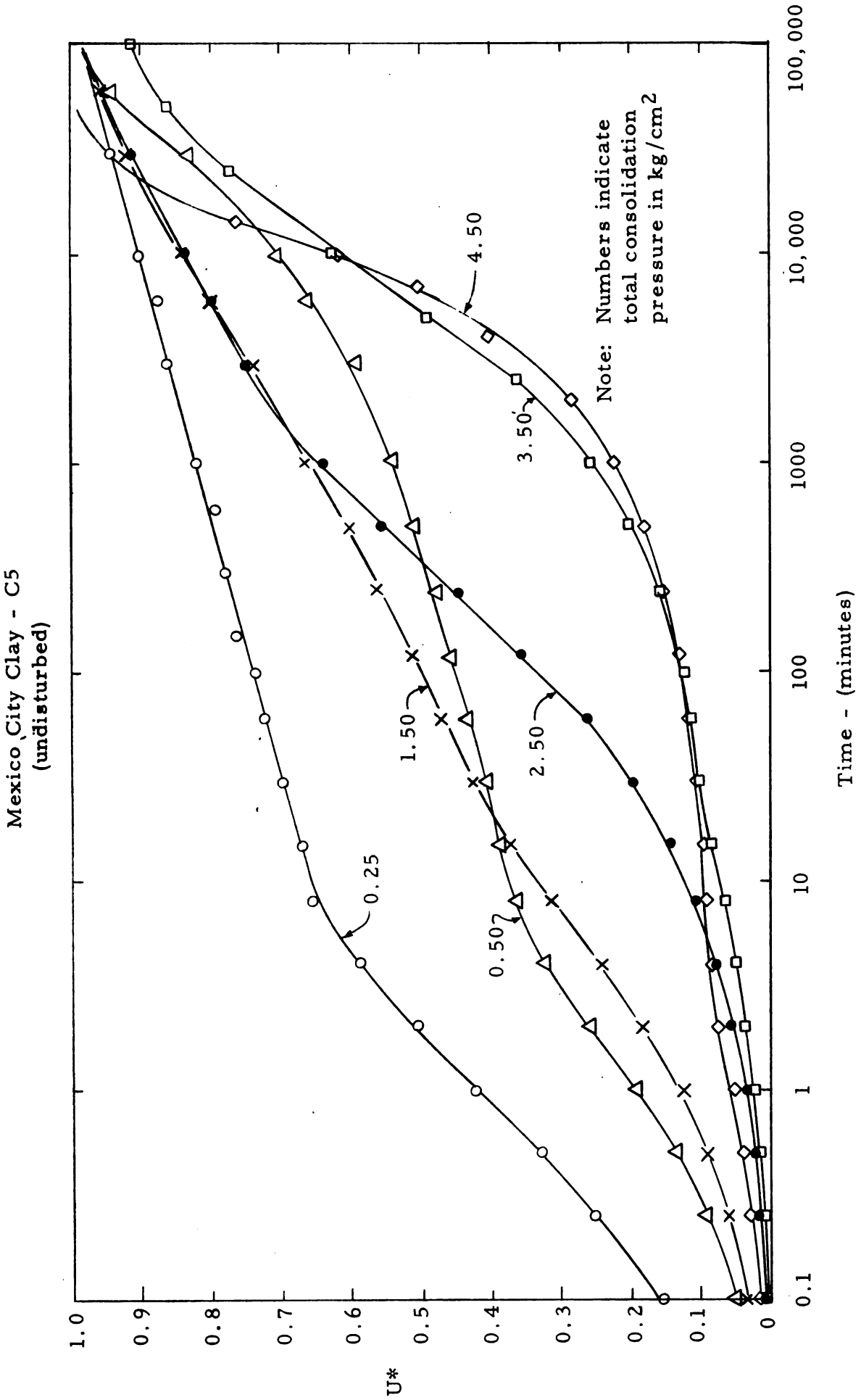
Mexico City Clay - C5
(undisturbed)
U*
Time - (minutes)
0.1
1
10
100
1000
10,000
100,000
0
0.1
0.2
0.3
0.4
0.5
0.6
0.7
0.8
0.9
1.0
0.25
0.50
1.50
2.50
3.50
4.50
Note: Numbers indicate
total consolidation
pressure in kg/cm2

APPENDIX C

CALCULATED PARAMETERS

TEST RESULTS

1. Clay - Marine City (undisturbed)
   Sample 1

Load Inc. (kg/cm^2)	k_1 (kg/cm^2)	k_2 (kg/cm^2)	$\frac{k_1}{k_1+k_2}$	$\alpha\beta_2$ ($cm^2/kg\text{-}min$)	α (cm^2/kg)	β $10^{-7}(min^{-1})$
0 - 0.625	3.55	26.0	0.12	8.20 $\times 10^{-5}$	300	2.73
0.625 - 1.25	3.76	13.3	0.22	3.53	235	1.52
1.25 - 2.50	5.81	21.6	0.24	2.77	107	2.59
2.50 - 5.00	21.6	26.4	0.45	.050	75.5	.066
5.00 - 10.00	39.1	44.0	0.47	.068	20.4	.333

2. Clay - Marine City (remolded)
   Sample 2a

Load Inc. (kg/cm^2)	k_1 (kg/cm^2)	k_2 (kg/cm^2)	$\frac{k_1}{k_1+k_2}$	$\alpha\beta_2$ ($cm^2/kg\text{-}min$)	α (cm^2/kg)	β $10^{-8}(min^{-1})$
0 - .031	1.17	1.05	0.53	260 $\times 10^{-5}$	1060	246
.031 - .0625	7.12	2.50	0.74	10.8	850	12.7
.0625 - .125	0.46	1.37	0.36	3.89	587	6.63
.125 - .250	0.68	1.74	0.28	2.64	559	4.73
.250 - .500	2.05	3.64	0.36	1.37	217	6.31
.500 - 1.00	2.84	5.06	0.36	0.105	179	0.59
1.00 - 2.00	5.26	8.60	0.38	0.301	84.6	3.56

3. Clay - Marine City (undisturbed)
   Sample 2b

Load Inc. (kg/cm^2)	k_1 (kg/cm^2)	k_2 (kg/cm^2)	$\frac{k_1}{k_1+k_2}$	$\alpha\beta_2$ ($cm^2/kg\text{-}min$)	α (cm^2/kg)	β $10^{-8}(min^{-1})$
.500 - 1.00	8.5	24.2	0.26	88.5 $\times 10^{-6}$	172.5	51.3
1.00 - 2.00	11.2	16.85	0.40	5.24	80.5	6.50
2.00 - 4.00	23.2	21.4	0.52	0.359	36.7	0.98
4.00 - 8.00	10.3	17.25	0.375	0.496	28.2	1.76
8.00 - 16.00	38.9	31.8	0.55	0.115	9.6	1.20

TEST RESULTS (cont'd)

4. Clay - Sault Ste. Marie (remolded)
Sample 1

Load Inc. (kg/cm^2)	k_1 (kg/cm^2)	k_2 (kg/cm^2)	$\frac{k_1}{k_1+k_2}$	$\alpha\beta_2$ (cm^2/kg-min)	α (cm^2/kg)	β $10^{-8}(min^{-1})$
0 - 0.156	2.22	3.18	0.40	33.8 $\times 10^{-6}$	421	8.03
0.312 - 0.625	1.87	3.18	0.37	19.3	168	11.5
0.625 - 1.25	2.47	5.25	0.32	11.6	97.5	11.9
1.25 - 2.50	3.48	7.39	0.32	6.78	56.0	12.1
2.50 - 5.00	4.36	14.6	0.23	8.96	45.7	19.6

5. Clay - Mexico City (undisturbed)
Sample A5

Load Inc. (kg/cm^2)	k_1 (kg/cm^2)	k_2 (kg/cm^2)	$\frac{k_1}{k_1+k_2}$	$\alpha\beta_2$ (cm^2/kg-min)	α (cm^2/kg)	β $10^{-8}(min^{-1})$
0 - 0.25	1.38	11.1	0.11	14.7 $\times 10^{-5}$	710	207
0.25 - 0.50	11.3	9.25	0.55	0.358	305	1.17
0.50 - 1.00	8.65	5.30	0.62	0.157	120	1.31
1.00 - 2.00	0.72	1.34	0.35	3.36	52.7	63.8
2.00 - 4.00	0.275	3.16	0.08	26.8	122	220
4.00 - 8.00	1.15	5.26	0.18	3.13	23.0	136

6. Clay - Mexico City (undisturbed)
Sample B1

Load Inc. (kg/cm^2)	k_1 (kg/cm^2)	k_2 (kg/cm^2)	$\frac{k_1}{k_1+k_2}$	$\alpha\beta_2$ (cm^2/kg-min)	α (cm^2/kg)	β $10^{-8}(min^{-1})$
0 - 0.25	1.89	9.2	0.17	256 $\times 10^{-5}$	459	55.8
0.25 - 0.50	7.45	7.45	0.50	1.55	258	6.0
0.50 - 1.00	7.62	3.92	0.66	0.106	97.8	1.08
1.00 - 1.50	8.70	1.30	0.87	1.06	60.4	17.6
1.50 - 2.00	31.2	1.08	0.968	2.29	46.4	49.4
2.00 - 2.50	19.3	1.23	0.94	0.404	41.3	9.8

TEST RESULTS (cont'd)

7. Clay - Mexico City (undisturbed)
Sample B5

Load Inc. (kg/cm^2)	k_1 (kg/cm^2)	k_2 (kg/cm^2)	$\frac{k_1}{k_1+k_2}$	$\alpha\beta_2$ (cm^2/kg-min)	α (cm^2/kg)	β $10^{-8}(min^{-1})$
0 - 0.25	1.04	9.40	0.10	733 $\times 10^{-6}$	662	111
0.25 - 0.50	5.23	8.70	0.375	10.8	344	3.14
0.50 - 0.75	7.90	5.27	0.60	2.76	215	1.28
0.75 - 1.00	10.50	4.50	0.70	4.55*	291	1.56
1.00 - 1.25	14.9	2.63	0.85	3.18	106	3.00
1.25 - 1.50	23.2	1.55	0.938	9.45	58.5	15.9
1.50 - 1.75	22.6	0.82	0.965	6.72	17.6	38.2

8. Clay - Mexico City (undisturbed)
Sample C5

Load Inc. (kg/cm^2)	k_1 (kg/cm^2)	k_2 (kg/cm^2)	$\frac{k_1}{k_1+k_2}$	$\alpha\beta_2$ (cm^2/kg-min)	α (cm^2/kg)	β $10^{-7}(min^{-1})$
0 - 0.25	2.07	4.40	0.32	5.85 $\times 10^{-5}$	525	1.11
0.25 - 0.50	5.12	3.14	0.62	0.730	145	0.503
0.50 - 1.50	3.66	2.54	0.59	0.50	71	0.705
1.50 - 2.50	11.9	1.32	0.90	2.08*	29.1	7.15
2.50 - 3.50	21.4	2.38	0.90	1.68	16.9	9.95
3.50 - 4.50	32.7	3.52	0.90	2.04	4.92	41.5

* $\alpha\beta_1$

APPENDIX D

VARIATION OF α, β AND $\frac{k_1}{k_1 \ k_2}$ FOR INCREASING STRESS - GRAPHICAL

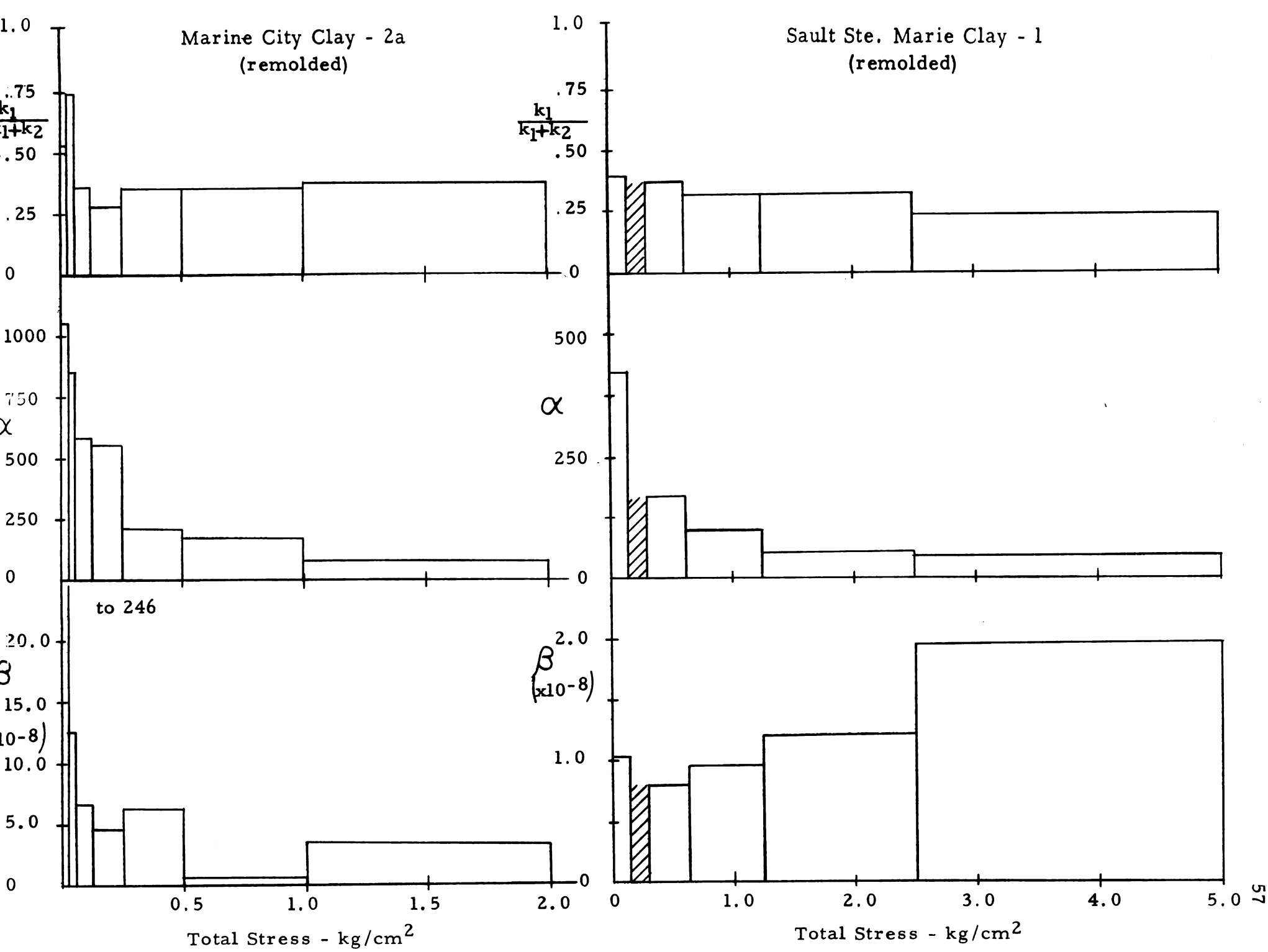
Marine City Clay - 2a
(remolded)
Sault Ste. Marie Clay - 1
(remolded)
1.0
.75
.50
.25
0
$\frac{k_1}{k_1+k_2}$
1000
750
500
250
0
α
to 246
20.0
15.0
10.0
5.0
0
β
$(\times 10^{-8})$
500
250
2.0
1.0
0.5
1.0
1.5
2.0
3.0
4.0
5.0
Total Stress - kg/cm^2

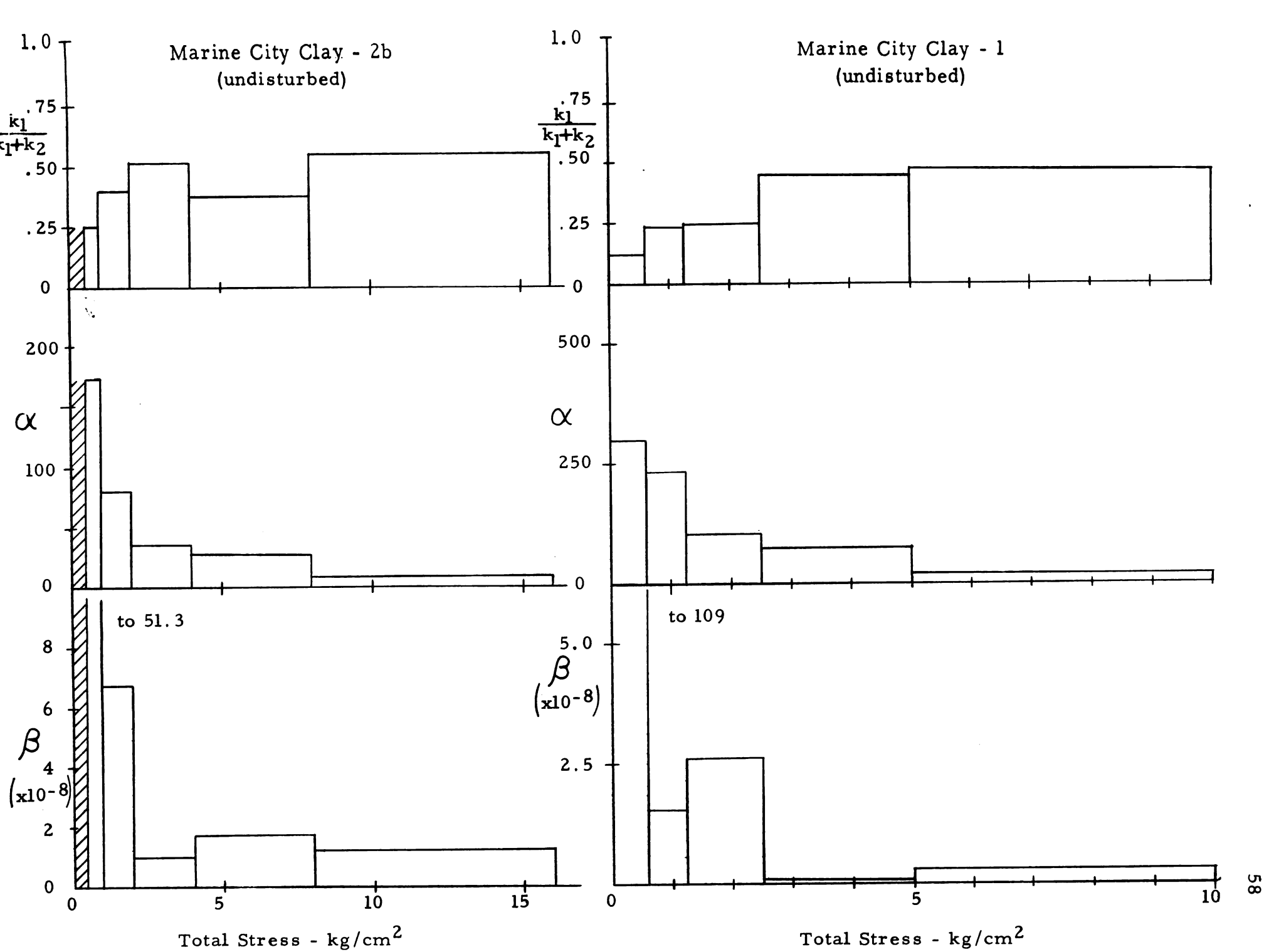
Marine City Clay - 2b
(undisturbed)
Marine City Clay - 1
(undisturbed)
$\frac{k_1}{k_1+k_2}$
1.0
.75
.50
.25
0
200
100
α
to 51.3
8
6
4
2
β
(x10⁻⁸)
5
10
15
Total Stress - kg/cm²
500
250
to 109
5.0
2.5

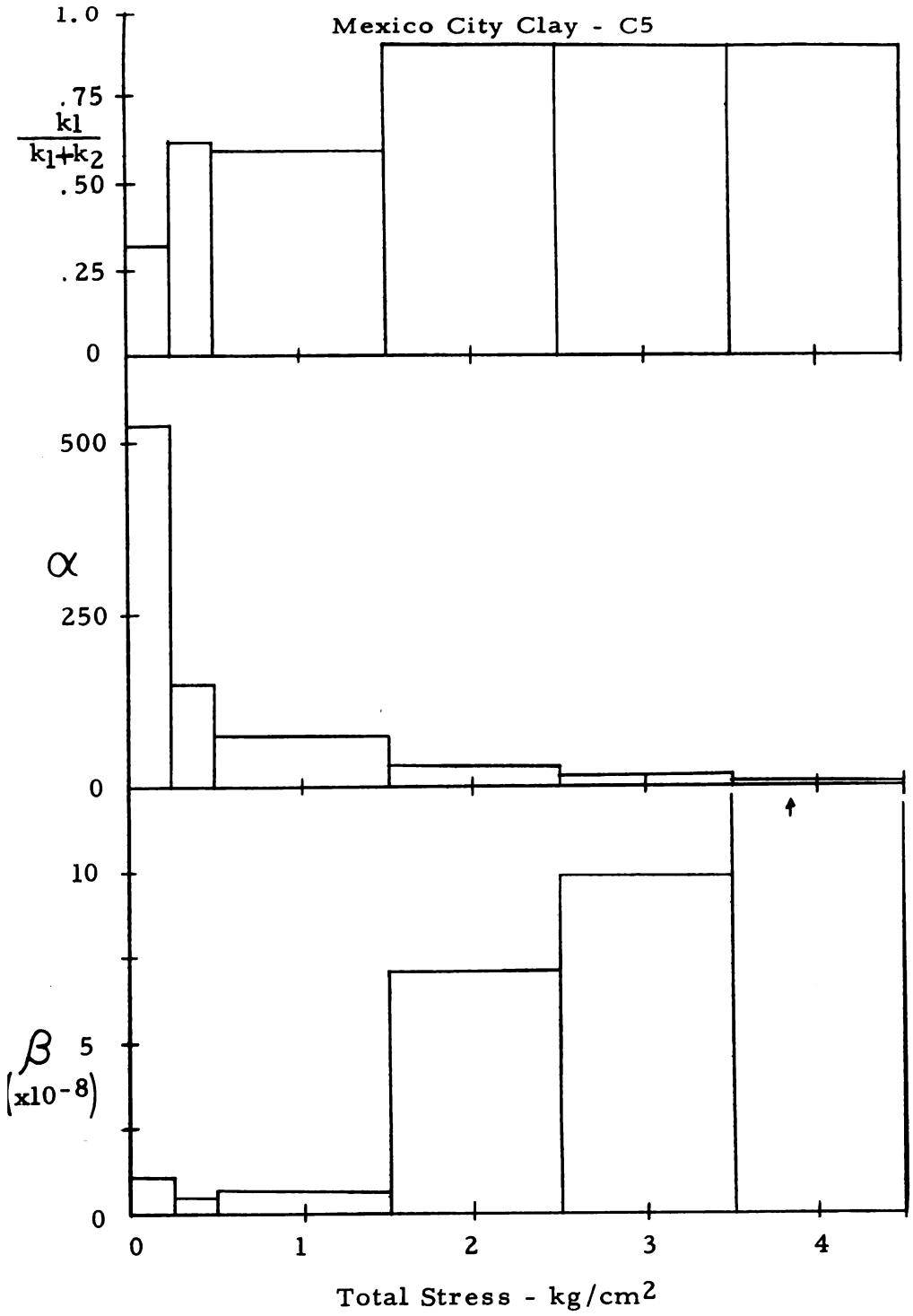
Mexico City Clay - C5
1.0
.75
$\frac{k1}{k_1+k_2}$
.50
.25
0
500
α
250
0
10
β 5
$(x10^{-8})$
0
0
1
2
3
4
Total Stress - kg/cm^2

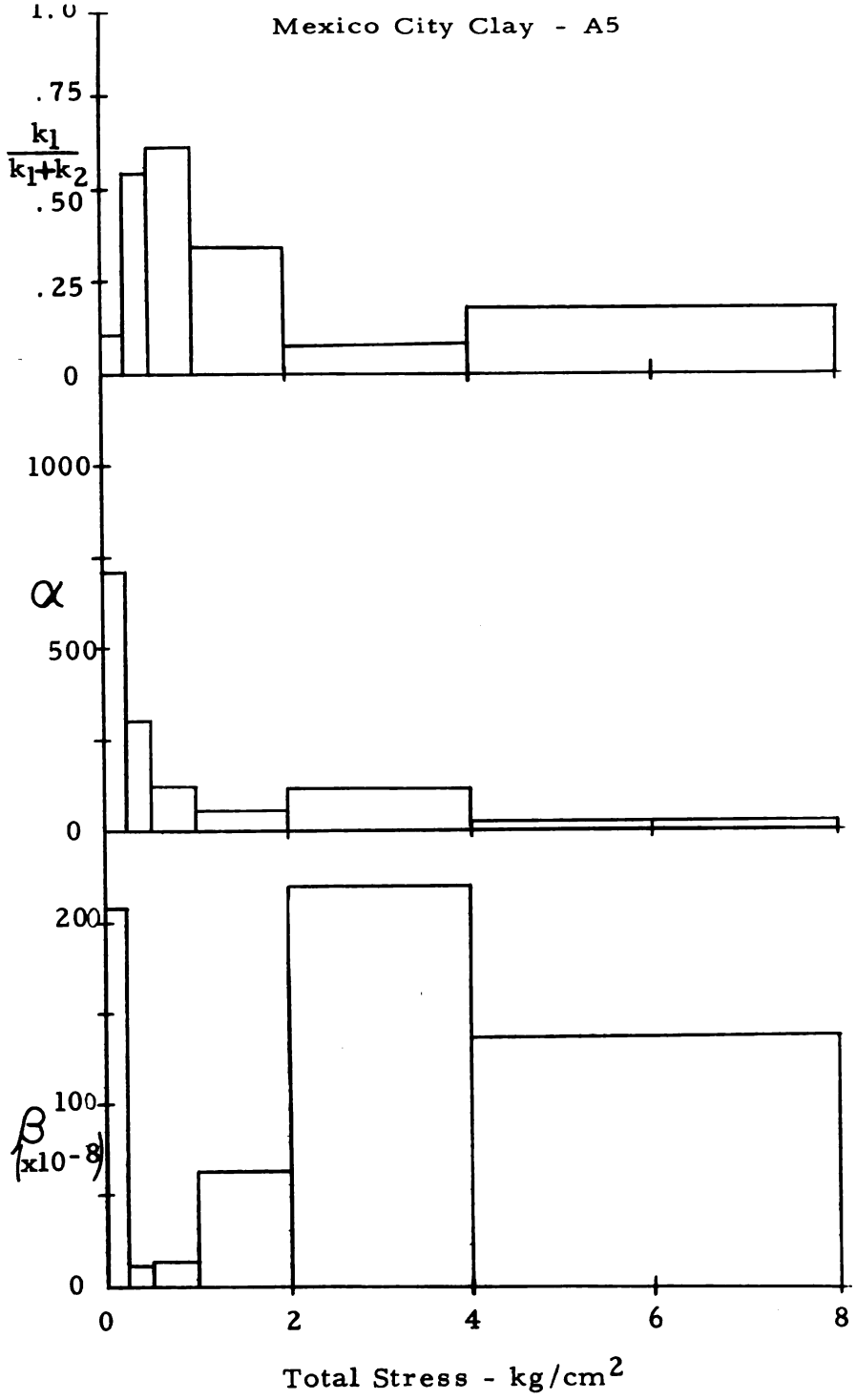
Mexico City Clay - A5
1.0
.75
$\frac{k_1}{k_1+k_2}$
.50
.25
0
1000
α
500
0
200
100
β
$(x10^{-8})$
0
0
2
4
6
8
Total Stress - kg/cm^2

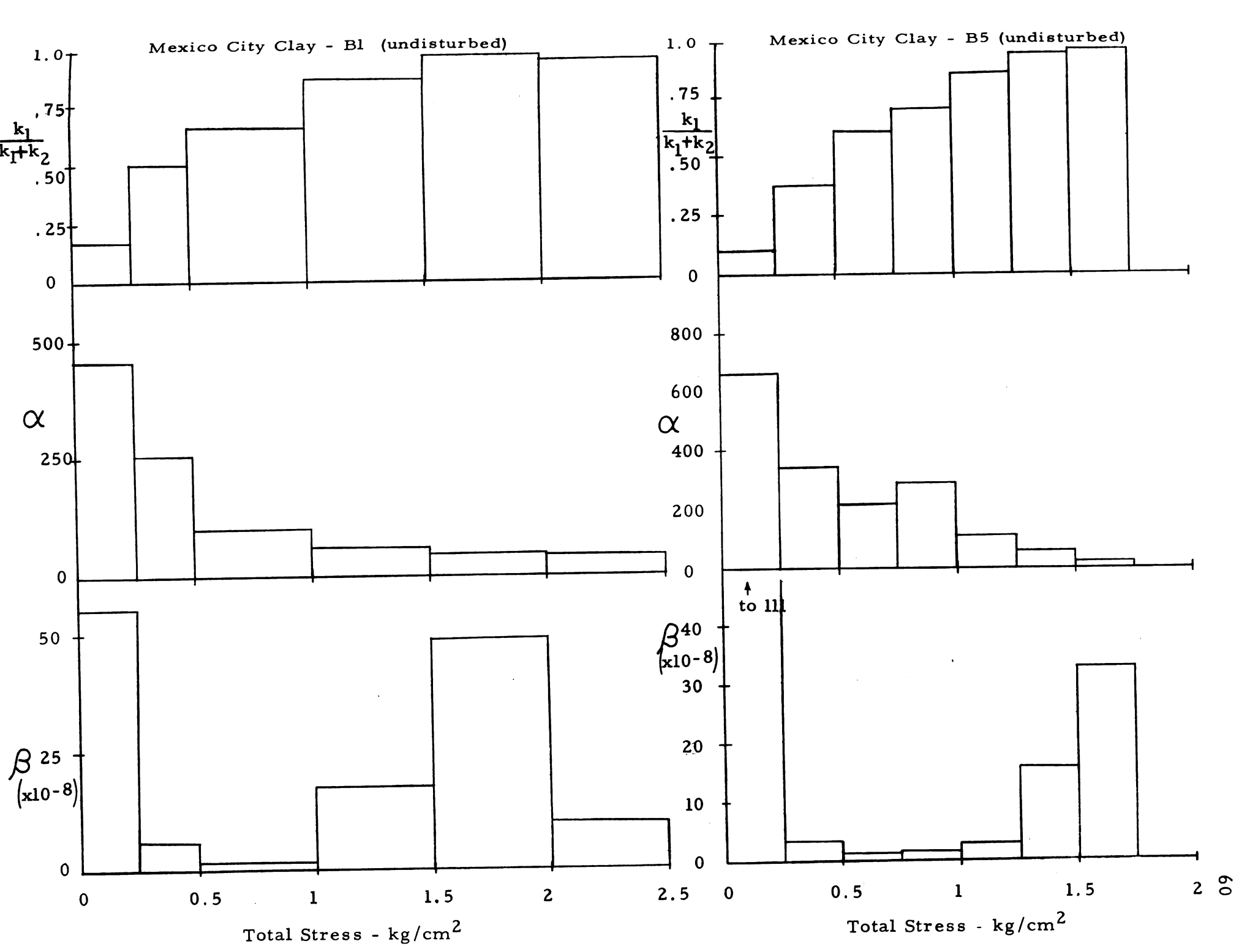
Mexico City Clay - B1 (undisturbed)
Mexico City Clay - B5 (undisturbed)
$\frac{k_1}{k_1+k_2}$
1.0
.75
.50
.25
0
α
500
250
800
600
400
200
to 111
β (x10-8)
50
25
40
30
20
10
0
0.5
1
1.5
2
2.5
Total Stress - kg/cm2
60

APPENDIX E

SAMPLE CALCULATIONS

SAMPLE CALCULATIONS

Clay - Marine City (undisturbed)
Sample 1
Pressure - 2.50 kg/cm^2 Increment - 1.25 kg/cm^2

See figure Ea for plot of test data. Figures Eb and c are used to evaluate U_∞. We found U_o by plotting U vs. t (for small t) arithmetically and projecting the resulting curve back to its zero intercept.

C_v is calculated to be 2.32×10^{-2} in^2/min.

$\bar{p}/p_o$ vs. t is plotted in figure Ed.

Take several small increments of Δt and plot $\Delta U^*/\Delta(\bar{p}/p_o)$ vs. t. Extending this line to its intersection with t=0 yields $k_2/(k_1+k_2) = 0.76$ (figure E1).

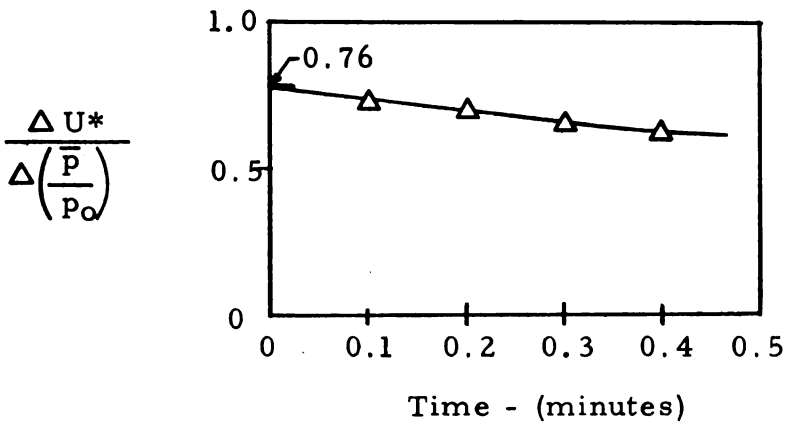

Figure E1. Determination of $k_2/(k_1+k_2)$

$$k_2 = \frac{p_o}{4(\epsilon_1)_\infty} = \frac{1.25}{4 \times 0.0144} = 21.6 \text{ kg/cm}^2$$

$$k_1 = \frac{21.6 \times 0.24}{0.76} = 5.81 \text{ kg/cm}^2$$

$$m^* = \frac{92.5 - 85.0}{\log 1000 - \log 100} = 7.5/\text{cycle}$$

$$m^{**} = m^* \left(\frac{k_1+k_2}{k_1}\right) = \frac{7.5}{.24} = 31.3/\text{cycle}$$

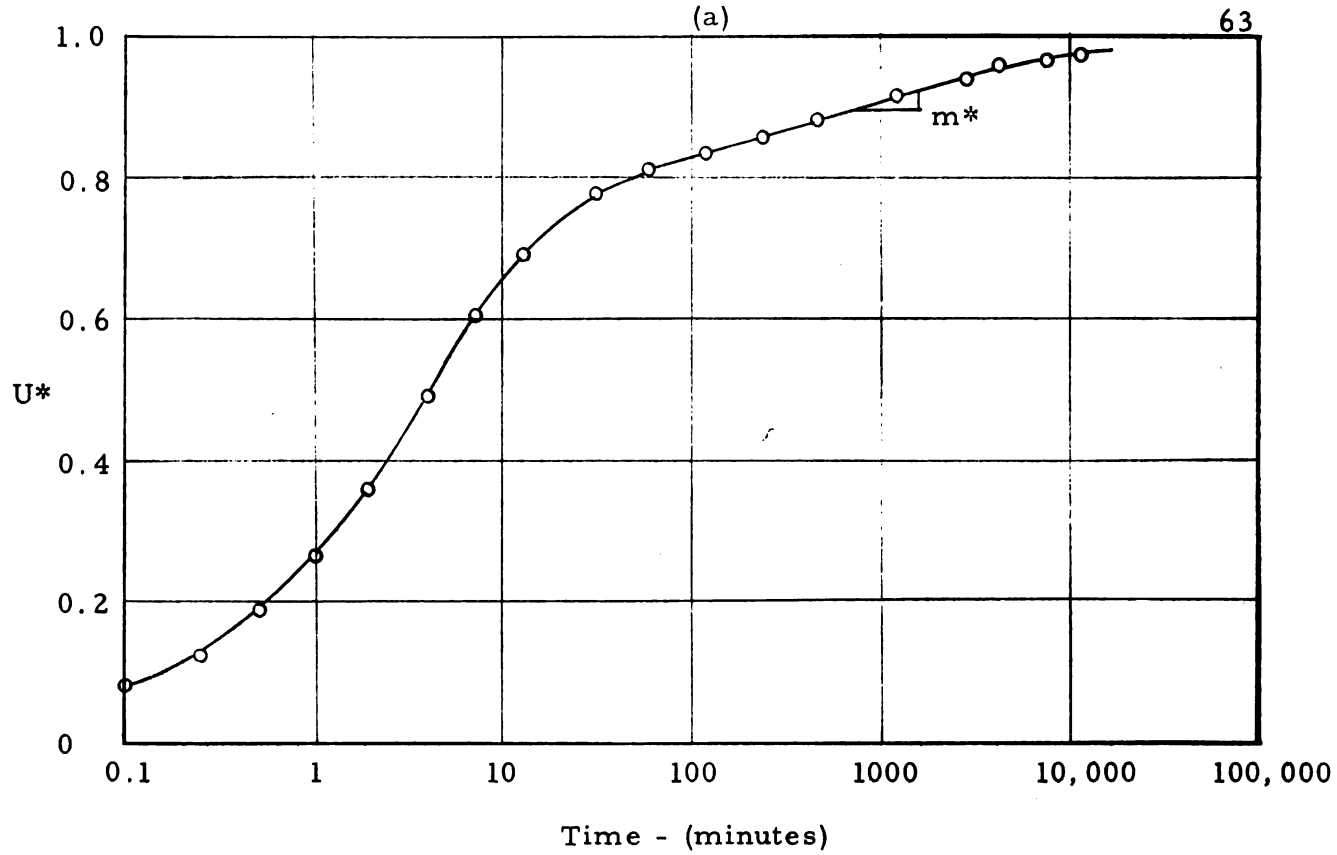
(a)
1.0
0.8
0.6
0.4
0.2
0
U*
m*
0.1
1
10
100
1000
10,000
100,000
Time - (minutes)

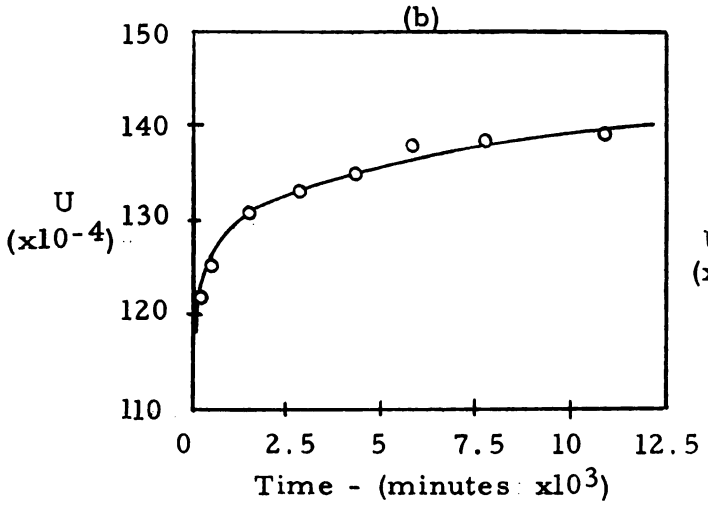
(b)
150
140
130
120
110
U
(x10-4)
0
2.5
5
7.5
10
12.5
Time - (minutes x10³)

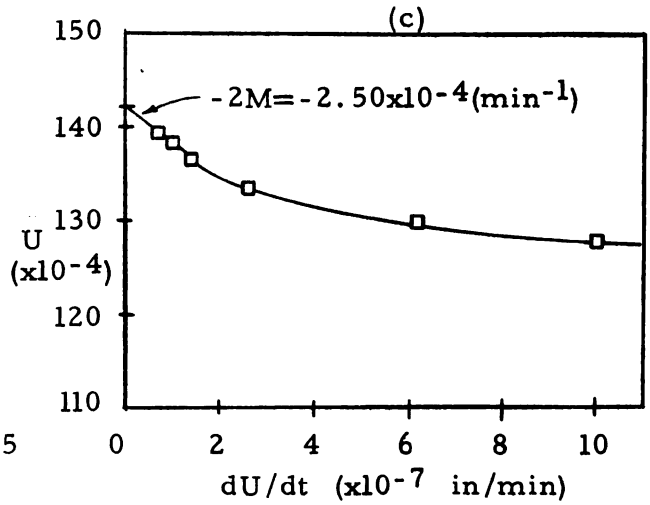
(c)
150
140
130
120
110
U
(x10-4)
-2M=-2.50x10-4(min-1)
0
2
4
6
8
10
dU/dt (x10-7 in/min)

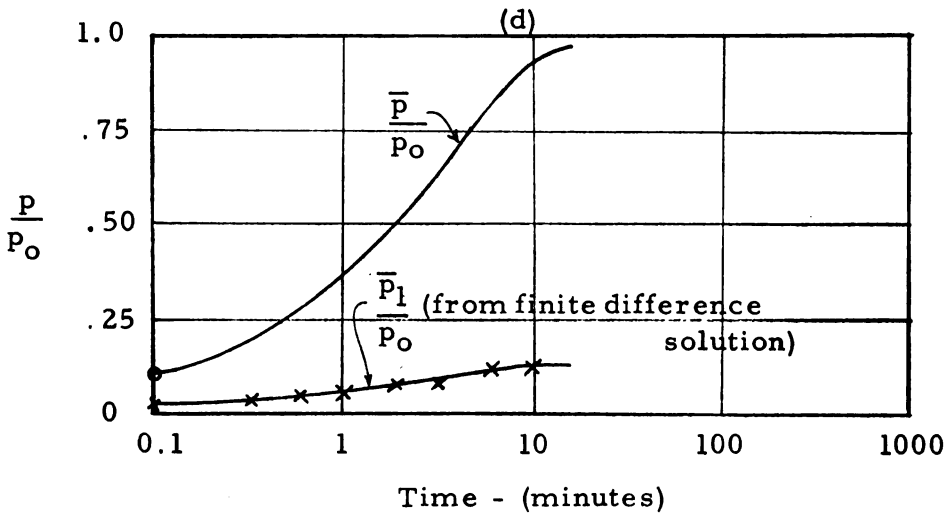
(d)
1.0
.75
.50
.25
0
P/Po
P̄/Po
P̄1/Po (from finite difference solution)
0.1
1
10
100
1000
Time - (minutes)

Figure E

therefore $A = 7.60$ (from figure 4)

$$\frac{Z(t)}{t} = \frac{1.6\times10^{-2}}{250} = 6.4\times10^{-5}$$

$$\alpha\beta_2 = 2\frac{Z(t)}{t}\left(\frac{k_1 k_2}{k_1+k_2}\right) = 2(6.4\times10^{-5})\,(.218) = 2.77\times10^{-5}$$

Note: $\alpha\beta_{1,2}$ refer to the two methods for calculating this quantity.

The slope of the $\frac{d\dot{U}}{dU}$ curve in figure Ec gives us a value of $-2M = 2.50\times10^{-4}$

$$\alpha\beta_1 = -2M\,\frac{k_1\ k_2}{k_1+k_2} = 2.50\times10^{-4}\,(.218) = 5.35\times10^{-5}$$

$$\alpha = 3\sqrt{2}\left(\frac{A}{p_o}\right)\frac{k_1+k_2}{k_1} = 107 \quad cm^2/kg$$

$$\beta = \frac{\alpha\beta_2}{\alpha} = \frac{2.77\times10^{-5}}{107} = 2.59\times10^{-7} \quad min^{-1}$$

The calculations above and the figures in Appendix A indicate that the two methods described previously for calculating $\alpha\beta$ differ by a factor of two. Because of the approximations and estimates made in each of the methods, agreement is considered good if the ratio of the smaller to the larger of these corresponding values is less than 3.

In cases where the ratio exceeds 3, the author has used $\alpha\beta_2$ for calculations, having more confidence in the reliability of this method.